Oxygen-induced stress reveals context-specific gene regulatory effects in human brain organoids

Benjamin D. Umans[1], Yoav Gilad[1,2]*

1. Department of Medicine, Section of Genetic Medicine, The University of Chicago, Chicago, IL 60637, USA
2. Department of Human Genetics, The University of Chicago, Chicago, IL 60637, USA

Correspondence should be addressed to YG (gilad@uchicago.edu)

Abstract

The interaction between genetic variants and environmental stressors is key to understanding the mechanisms underlying neurological diseases. In this study, we used human brain organoids to explore how varying oxygen levels expose context-dependent gene regulatory effects. By subjecting a genetically diverse panel of 21 brain organoids to hypoxic and hyperoxic conditions, we identified thousands of gene regulatory changes that are undetectable under baseline conditions, with 1,745 trait-associated genes showing regulatory effects only in response to oxygen stress. To capture more nuanced transcriptional patterns, we employed topic modeling, which revealed context-specific gene regulation linked to dynamic cellular processes and environmental responses, offering a deeper understanding of how gene regulation is modulated in the brain. These findings underscore the importance of genotype-environment interactions in genetic studies of neurological disorders and provide new insights into the hidden regulatory mechanisms influenced by environmental factors in the brain.

Introduction

Understanding how gene regulatory variants function across different cellular and environmental contexts is essential for interpreting genetic associations with disease. Gene-by-environment (GxE) interactions occur when genetic variants influence how individuals respond to specific environmental exposures, leading to inter-individual differences in phenotypes, including variability in disease susceptibility. This concept is particularly important in complex diseases, where individuals with different genetic backgrounds may exhibit varying risk profiles for conditions such as neuropsychiatric disorders [1,2]. For instance, environmental factors such as stress [3–5], oxygen deprivation [6,7], or infection [8–13] can trigger disease-relevant gene regulatory effects that remain hidden in static, steady-state conditions.

Gene regulatory catalogs like GTEx (Genotype-Tissue Expression project [14]) provide valuable insights into how genetic variants affect gene expression across various tissues in steady-state conditions. However, the majority of disease-associated loci remain unexplained, likely due to their regulatory effects being specific to certain cell types or environmental contexts that have not been fully explored [15,16]. This gap is particularly pronounced in the brain, where the complex interplay between different cell types and environmental stressors can contribute to the onset and progression of neurological and psychiatric diseases [17–22].

Brain cells, especially neurons, are highly sensitive to environmental perturbations like hypoxia (oxygen deprivation), given the brain's high metabolic demand and susceptibility to oxidative damage [23]. Hypoxia is a well-known neurological risk factor throughout life, arising from conditions such as sleep apnea, high altitude, respiratory infections, and premature birth [24–28]. Hypoxic exposure has profound effects on cognitive function, white matter integrity, and increase the risk for neurodegeneration and psychiatric disorders [29–47]. Despite the importance of oxygen homeostasis and hypoxia to brain function, we lack comprehensive insight into how different brain cell types respond to these environmental stressors at the gene regulatory level, which limits our ability to interpret genetic associations with neurological traits [47–50].

In this study, we used human brain organoids to investigate the transcriptional responses of diverse brain cell types to oxygen perturbation across 21 individuals. By applying single-cell RNA sequencing, we captured gene expression data both under baseline conditions and after exposure to varying oxygen levels. Through whole-genome sequencing of each donor, we identified genetic contributions to these responses, revealing dynamic gene regulatory effects with significant relevance to neurological and psychiatric disease susceptibility. This approach goes beyond characterizing gene regulatory variation in static, post-mortem tissue and opens new avenues for studying GxE interactions in a controlled, *in vitro* setting.

Results

We differentiated brain organoids from the iPSCs of 21 unrelated Yoruba individuals from Ibadan, Nigeria [51] (see Methods). We performed oxygen manipulation experiments in two batches of 7-16 individuals, with two individuals replicated across batches to allow us to control and account for batch effects (**Figure 1a**). Specifically, following seven weeks of growth at atmospheric oxygen levels (21% O_2), organoids were adapted to 10% O_2 to mimic the physiologic environment experienced by brain cells *in vivo*. After one week of culture at 10% O_2, organoids were either maintained at physiologic oxygen (baseline/normoxia), transferred to low oxygen (1% O_2; hypoxia), or transferred to high oxygen (21% O_2; hyperoxia) for 24 hours. Following the treatments, we dissociated organoids in the presence of transcriptional inhibitors and multiplexed equal proportions of each sample in preparation for single-cell RNA-sequencing, targeting 3,000 cells per individual and oxygen condition, and a depth of 20,000 reads per cell. After demultiplexing and quality control, we retained data from 170,841 cells (normoxia: 52,671, hypoxia: 57,788, hyperoxia: 60,382; median 5,666 UMI counts per cell).

Brain organoids comprise diverse cortical and non-cortical cell types

We first sought to characterize the cell type composition of brain organoids maintained at baseline oxygen levels. We annotated cell clusters using fetal brain reference data and known marker genes [52,53], finding a variety of cortical cell types, including radial glial progenitors, intermediate progenitors, excitatory neurons, and inhibitory neurons (**Figure 1b, S1**, **Methods**). We also identified a substantial cluster of neurons with non-cortical identities, including thalamic and midbrain inhibitory neurons and $GNRH^+$ cells (**Figure 1b, S1,** Methods). Out of 20 high-confidence cell types, 10 are present in over half of the individuals, with a median of 11 cell types detected per individual (**Figure 1c**).

We used *propeller* [54] to assess differences in cell type proportions across treatment conditions, and found that organoid composition was largely unaltered by oxygen manipulation (**Figure S2a, Table S1**). Moreover, the cell type composition of an additional set of control organoids which we maintained at atmospheric oxygen levels for the duration of the experiment did not differ substantially from what we observed in the treatment conditions (**Figure S1b**). We observed differences in cell type composition across individuals, with the rarer cell types (such as midbrain dopaminergic-like cells, mature oligodendrocytes, vascular leptomeningeal cells, and Cajal-Retzius cells) present in only a minority of samples (**Figure 1, S1e**). However, across treatments, the cell type composition of organoids from the same individuals generally remained similar (with the exception of NA19144; **Figure S2a**), suggesting that the treatments did not have a marked effect on cellular composition.

Since the treatments did not seem to result in noticeable differences in cell composition, we focused again on the differences in cell composition across individuals. We found no effect of sex or iPSC passage number on cell type proportions, but we observed that certain rare cell types – including oligodendrocytes, inhibitory neuron subtypes (midbrain, thalamic, and SST^+), and midbrain dopaminergic-like cells – differed in proportion across individuals from different collection batches (**Table S1**). To assess the extent of confounding by batch, we merged biologically similar clusters to generate a set of 10 coarse annotations representing the principal cell types in our data (**Figure S1d, Methods**). When we examined cell type proportions among coarsely-defined clusters, the batch effect disappeared, suggesting that principal cortical cell types were largely stable across experiments. Still, we performed all subsequent analyses using both annotations to assess potential bias caused by over clustering (**Methods**), and to ensure that the two approaches produce similar outcomes. In what follows, we report findings from the more interpretable fine-grained annotation set (results from the coarse clustering approach are provided in **Figure S1d, S1e, S2d-e, S4a, S4b, S5b-f**).

Shared transcriptional response patterns reveal cell-type-specific vulnerabilities to hypoxia

To identify differentially expressed (DE) genes between baseline and either hypoxic or hyperoxic conditions, we applied a linear mixed model to pseudobulk expression data for each cell type and treatment condition[55]. We identified a total of 10,230 DE genes in response to hypoxia, ranging from 91 to 5,590 genes per cell type (FDR<0.05, **S Table S2**). Similarly, we identified 10,425 hyperoxia-responsive genes, ranging from 17 to 6,102 genes per cell type (FDR<0.05, **S Table S2**). In at least one (any) cell type, 2,703 hypoxia-responsive genes (and correspondingly, 2,855 hyperoxia-responsive genes)

exhibited a greater than 1.5-fold change in expression compared to baseline. As expected, we detected far more DE genes in abundant cell types (**Figure S2c**), within which 76-92% of hypoxia-evoked transcriptional effects and 84-93% of hyperoxia-evoked transcriptional effects were modest (smaller than 1.5-fold).

We were intrigued by the large differences in the numbers of DE genes across cell types, an observation that cannot be fully explained by cell abundance (Figure S3). To explore this further, we analyzed the data using multivariate adaptive shrinkage (*mash*) [56], to account for incomplete power and assess the similarity of transcriptional responses across treatment conditions and cell types. By combining power across cell types, we were able to detect weak DE effects that emerge in multiple cell types and, importantly, accurately identify condition- and cell-type-specific DE genes.

As expected, we observed similar oxygen response patterns among related cell types (**Figure 2a**). Even using *mash*, we found that more than half of the oxygen-responsive genes we identified (68% of hypoxia-responsive genes and 63% of hyperoxia-responsive genes, FDR<0.05, effect size >1.5-fold) were DE in fewer than three cell types, consistent with the idea that oxygen homeostasis mechanisms are tuned to the needs of distinct brain cell types [57]. We also observed a tendency for DE genes with large effects to be more cell-type-specific than DE genes with smaller effects (**Figure S2b**), an observation that is counter-intuitive with respect to power considerations.

Most cell types exhibited a modest positive correlation between the transcriptional responses to hypoxia and hyperoxia (**Figure 2a, S2**), and many gene families related to general response to stress were enriched among DE genes in both treatment conditions. For example, all oxygen-treated cell types are enriched for DE genes with roles in cellular metabolism and inflammation, and most are enriched for DE genes involved in cell proliferation and apoptosis (**Figure 2b**). Reassuringly, hypoxia, specifically, also induced a well-recognized core regulatory program across all cell types, including the upregulation of hypoxia-inducible factor (HIF) target genes [58–60].

As our observations pointed to a general stress response following the treatments, we sought to characterize the proportion of single cells expressing regulatory signatures of stress in baseline and treatment conditions, so we can specifically focus on the response to the treatments. To parse cell type heterogeneity in the transcriptional response to oxygen perturbation, and to differentiate between stressed and unstressed cells, we identified gene sets that capture robust and general responses to each treatment condition (**Table S3, Methods**). We leveraged these gene sets in a granular filtering approach [61] to classify cells as either stressed or unstressed, and then repeated our differential expression analysis after censoring the stressed cells. We found that although stressed cells contribute disproportionately to the treatment expression response, they do not account for it entirely: in cell types with a higher proportion (12-36%) of stress-censored cells, the number of DE genes (FDR<0.05, fold-change>1.5) decreased by as much as 64% relative to randomly censored data (**Figure S4d**).

Cell types that include an increased fraction of stressed cells following exposure to hypoxia or hyperoxia may be especially sensitive to oxygen perturbation. We calculated the change in the proportion of stressed cells between baseline and treatment conditions to assess cell-type-specific sensitivity within brain organoids. We found that intermediate progenitors, immature neurons, and radial glia are particularly responsive to both hypoxia and hyperoxia (**Figure 2c, S4**).

The observation of large differences in cell-type sensitivity to changes in oxygen may be significant and help us better understand disease mechanisms. It is possible, however, that cell-type-specific sensitivity to the treatments could be explained by variation in organoid spatial structure. To examine this, we used antibody markers to map eight major cell types in cryosections obtained from the same organoids we used for sequencing (**Methods**). We then quantified the accessibility of each cell type to exogenous oxygen by measuring the distance from immunostained cells to the organoid periphery and compared the distance distribution across cell types. While different cell types were distributed at various depths within each organoid, variation between organoids was comparable to the differences observed between cell types (**Figure 2d**; ANOVA F-test of organoid-level medians, p=0.342). On the whole, the most oxygen-sensitive cell types were localized neither more superficially nor more deeply than other cell types. Thus,

cell type-specific sensitivity to oxygen perturbation appears to be driven primarily by cellular identity, rather than cell position within the organoids.

Context-specific responses to oxygen perturbation

We observed that oxygen perturbation induced widespread transcriptional effects, many of which were shared among subsets of cells within and between cell types. Perturbed cells continued to express cell-type-specific markers, simultaneously maintaining their respective identities while adopting a more general signature of oxidative stress (**Figure S4c**). This suggests that discrete cell types may fail to capture continuous contextual responses, including signatures shared by developmentally related or physically proximal cells. In an effort to capture the subtler transcriptional patterns in our data, we used topic modeling to decompose cellular transcriptomes into 15 groups (topics) that capture distinct sources of transcriptional variation (**Methods**).

Several topics largely recapitulate discrete cell type classifications, as expected, consistent with the notion that cell identity is the primary source of transcriptional heterogeneity in our data (**Figure 2e**). Other topics, such as topic 7, recapitulate properties that were already known to us, such as the collection of DE genes that we previously used to identify hypoxia-stressed cells (**Figure S3d**). We also identified topics that captured dynamic cellular processes and developmental states. Still, several topics revealed new patterns: topic 4 is shared by dividing radial glia and dividing intermediate progenitors and is distinct from separate topics that tightly correlate with each of these cell identities in isolation. Indeed, topic 4 is defined by elevated expression of genes involved in DNA replication and cell division, including *MKI67*, *TOP2A*, and centrosomal proteins (**Figure S3d**), capturing shared aspects of the dividing cell environment across different cell types. In turn, topic 3 shows modest loading in cortical hem progenitors and higher loading in choroid plexus cells, reflecting their shared developmental origins: signals from the cortical hem influence the differentiation and patterning of cells at the boundary of the cerebral cortex and hippocampus, including those forming the choroid plexus [62]. Altogether, topic modeling allowed us to recapture functional relationships and shared states that were concealed in our analysis of discrete, mutually-exclusive cell type clusters, providing us with an enriched view of brain organoid dynamics.

Transcriptional responses to oxygen perturbation are genetically regulated

Having detected thousands of genes that are differentially expressed in response to oxygen perturbation, we sought to uncover potential genetic sources for inter-individual variation in treatment response. We aggregated single-cell gene expression data into pseudobulk groups defined by their unique combination of donor, cell type, and treatment condition. After excluding groups comprising fewer than 20 cells, we removed cell types that had fewer than seven individuals in each treatment condition (**Methods**). For each of the 14 remaining cell types, we separately mapped *cis* eQTLs under hypoxic, hyperoxic, and baseline conditions, including gene expression principal components as model covariates to account for the effects of sex, batch, and latent confounding factors (**Methods**). We expected most eQTLs to be shared across treatment conditions – indeed, our DE analysis indicates that most genes are robust to oxygen perturbation. We therefore used *mash* to weigh evidence for SNP-gene associations across all three treatment conditions, considering each cell type in turn. As we and others have found, this approach improves power to detect individually weak signals that emerge consistently in multiple experimental contexts [63–65].

Across 14 cell types, we tested a total of 9,478 genes and found 36,778 *cis* eQTLs in 8,320 genes, with a median of four eQTLs per eGene (local false sign rate < 0.05). Among these, we identified 14,358 standard eQTLs (in 5,952 eGenes), in which the eQTL effect size is of similar size and direction across all treatment conditions (we used a conservative 2.5-fold cutoff to define similar effect sizes across treatment conditions, as we consider shared effects to be the null; **Table S4**). We also identified 22,420 oxygen-response eQTLs in 7,338 genes, namely eQTLs that have significantly different effect sizes between treatment conditions. Note that the sum of eGenes associated with at least one standard eQTL and those associated with at least one oxygen-responsive eQTLs is larger than 8,320, because eGenes are often

associated with more than a single eQTL across cell types, and often with both standard and eQTL oxygen-responsive eQTLs in different cell types

Oxygen-responsive eQTLs included 3,687 loci associated with distinct effects in the hypoxia condition (in at least one cell type), 3,603 loci associated with distinct effects in hyperoxia, and 2,935 loci associated with a difference between the baseline normoxia and both treatments (**Figure 3a**). Of particular note, across cell types, 15,045 oxygen response eQTLs are not associated with a statistically significant eQTL in the baseline (normoxia) condition. The genetic effect of these loci on gene regulation in the different cell types can only be detected under the stress conditions imposed by the change in oxygen levels. Consistent with this, oxygen-responsive eQTLs – particularly those not found under normoxia – are associated with the expression of genes that are less likely to have eQTL effects in cerebral cortex tissues in GTEx (one-sided paired Wilcoxon test, P = 0.007; **Figure 3c, Figure S5a**).

Context-dependent genetic regulation

In the analysis of gene expression levels, topic modeling allowed us to place cells along continuous axes of variation that are not predicated upon marker gene or reference annotations. We reasoned that topics could also be deployed to identify genetic regulatory effects that emerge in contexts defined more precisely than is possible using the discrete categories of cell type and treatment. To explore the effects of *cis* eQTLs in an expanded set of precisely-defined cellular contexts, we tested for interactions between eQTLs and topics. Rather than individually testing each eQTL-topic interaction, we used CellRegMap [66] to jointly test all linear combinations of topics, improving our power to detect a wide range of genotype-context interactions.

We identified 289 genes with a topic-interacting eQTL. To infer the relevant cellular context for each eQTL, we assessed the correlation between its estimated effect and the loading for each topic. When possible, we checked to ensure our interpretation was corroborated by results from our analysis of discrete cell types and treatment conditions. For example, topic 15 describes cortical hem and glial progenitor cells. Out of the top 12 eGenes associated with topic 15 (Pearson correlation > 0.6), 10 were identified as eGenes exclusively in cortical hem or glial progenitor cells using our pseudobulk approach. Also, among the top 12 eGenes is the cholesterol transporter *ABCA1* (r = 0.77), which showed modest eQTL effects in our pseudobulk analyses of cortical hem cells, glial progenitors, radial glia, and intermediate progenitors (**Figure 4a**). Of note, radial glia are the precursors to both glial progenitors and intermediate progenitors. Concordantly, our topic-based approach revealed a modest correlation between *ABCA1* and topic 6 (r=0.26), which is defined primarily by radial glia.

Using the topic eQTL analysis we found 218 eGenes whose regulatory effects were significantly correlated with topic 7, which is associated with hypoxic stress ($p<0.05$, Bonferroni correction). Unexpectedly, 118 of these eGenes did not have hypoxia-specific eQTLs in our standard cell-type specific analysis, including *WDR45B* and *CD44*, which were more strongly correlated with topic 7 than any other topic. This is an example of the additional insight we can gain by using topics instead of discrete cell identities. *WDR45B* is a member of the WIPI protein family of autophagosomal proteins, and *WDR45B* mutations have been linked to numerous severe neurodevelopmental disorders [67]. *CD44* is a known regulatory target of HIF1 and interacts with HIF2 to modify local tissue responses to hypoxia [68,69]. While we identified multiple eQTLs for *WDR45B* using the standard analysis, they were either oxygen-insensitive or responsive specifically to *hyper*oxia. We also identified eQTLs for *CD44* that were oxygen-responsive, but not to hypoxia specifically. Taken together, these results highlight the utility of decomposing complex cellular states into constituent programs for the analysis of gene-by-environment interactions.

Context-dependent eQTLs help to interpret the effects of disease-associated loci

The use of brain organoids allowed us to identify context-specific gene regulatory effects that are underrepresented in standard eQTL studies of post-mortem tissues (**Figure 3c, Figure S5a**). We reasoned that oxygen-responsive eQTLs could help to explain uncharacterized genetic associations with disease – particularly if the eQTL effects were undetectable at baseline. To explore this possibility, we examined

the overlap of eGenes with GWAS loci assembled from 402 brain-relevant traits in each cell type (**Methods**). Across cell types, eGenes with response eQTLs that were latent at baseline (median 258.5 per cell type, 1,745 total) included a comparable number of disease-associated genes as standard eGenes detected at baseline (median 215 per cell type, 1,411 total; two-sided paired Wilcoxon test p=0.194; **Figure 4b**). Focusing on the 4,713 novel eGenes that were not represented in GTEx cerebral cortex tissues, we found an average of 158 disease-associated eGenes per cell type (total 1,014) to overlap oxygen-response eQTLs that were latent at baseline. Finally, of the 218 eGenes that interact with hypoxia (i.e., topic 7), 55 correspond to a GWAS gene, including 31 genes that are not eGenes in GTEx cortical tissue. Thus, mapping eQTLs in oxygen-treated brain organoids allowed us to uncover novel, disease-relevant effects that could not be detected in primary cortical tissues.

Next, we asked whether context-specific eQTLs could revise previous interpretation of disease-associated SNPs. Focusing on oxygen-responsive lead eQTL SNPs that were associated with brain traits in GWAS, we identified 146 associations (corresponding to 76 genes) in which eQTL mapping implicated a different target gene than the original GWAS report or a simple nearest-gene heuristic. For example, we identified a hyperoxia-specific association between rs2008012 and the expression of *H3F3B* in immature excitatory neurons and an oxygen-insensitive effect in dividing intermediate progenitors (**Figure 4c, Figure S5g**). rs2008012 is associated with variation in uncinate fasciculus white matter, which connects the limbic system to the brain's frontal lobes [70]. This SNP has been described as an eQTL for ten different genes, principally in blood, with brain data pointing to effects on expression of *TRIM47*, *TRIM65*, *WBP2*, and *ACOX1* [71–73]. While both coding and regulatory mutations in *H3F3B* are known to cause severe neurodevelopmental phenotypes, our data suggest that subtle, context-specific regulation of *H3F3B* expression during development may also contribute to microstructural brain features.

Most genes have been associated with at least one regulatory eQTL. However, protein-coding mutations are relatively rare. We reasoned that genes harboring rare deleterious coding mutations might also be regulated by common variants – albeit with subtler phenotypic effects. To determine whether context-specific eQTLs can be used to connect common GWAS variants with rare disease-causing mutations, we assembled results from five large exome studies of neurological or psychiatric traits, finding 1,672 genes with rare variants that are associated with at least one disease or developmental condition (**Methods**). Out of these 1,672 genes, 905 are eGenes in at least one cell type or condition in our data, and 349 have a significant GWAS association (**Figure 4d**). We identified 37 cases (corresponding to 22 genes) in which the lead SNP was significantly associated with a brain-related GWAS trait (**Table S5**). For example, damaging missense mutations in *ATP2A2* confer risk for bipolar disorder (OR 10.4) [74]. In subtypes of radial glia and mature neurons, we identified a novel eQTL for *ATP2A2* (rs4766428) that is strongly associated with cognitive ability, risk of schizophrenia, and risk of anorexia nervosa [75–78]. Similarly, a radial glial eQTL (rs9611486) for *EP300*—rare variants of which have been associated with autism, developmental delay, and Rubinstein-Taybi syndrome 2—is a risk SNP for anxiety symptoms [79,80]. Importantly, nearly half of the associations found in this comparison were not detected under baseline oxygen conditions, highlighting the importance of examining diverse cell types and perturbed states in order to identify trait-relevant regulatory effects.

Discussion

In this study, we measured cell-type-specific responses to oxygen stress in a genetically diverse panel of brain organoids. Oxygen perturbation induced a robust transcriptional response across all assayed cell types, which included a common oxygen stress response signature as well as cell-type-specific changes. Leveraging the genetic and cellular heterogeneity present in our organoid panel, we identified thousands of dynamic, oxygen-responsive eQTLs, many of which have effects that are undetectable at baseline and therefore are absent in data collected from post-mortem cortical tissues. Moreover, the use of topic modeling allowed us to identify genetic effects that transcend categorical notions of cellular identity to regulate cell division, differentiation, and other continuous processes. By collecting functional data from biological contexts that are difficult to access *in vivo*, we were able to characterize the putative regulatory role of hundreds of GWAS loci, many of which had never been associated with an eQTL. Our results show that repurposing organoids for gene-environment interaction studies is a valuable and increasingly

tractable approach that complements population genomic studies of primary tissues, and may be particularly valuable for studies of neurological and psychiatric diseases.

Our organoid differentiation approach included a small molecule cocktail designed to promote dorsal telencephalic patterning, which we selected to mitigate the between-organoid variability previously observed in un-patterned cortical organoids [81]. We nonetheless found substantial differences among organoids derived from different donor cell lines, with some cell types present in only a minority of samples. As expected, this cell type heterogeneity resulted in incomplete power to map eQTLs across cell types, reflecting the trade-off between cell type resolution and abundance inherent to single-cell data analysis. At the same time, this heterogeneity allowed us to measure gene regulation in biological contexts that have never before been examined at the population level.

Though all cell types in our study responded to hypoxia, intermediate progenitor cells were among the most sensitive to hypoxic challenge. Interestingly, immature neurons showed increased expression of the intermediate progenitor cell marker *TBR2*/*EOMES* following 24-hour hypoxia exposure, possibly indicating a rapid transition from intermediate progenitor to neuronal identity. Paşca et al. demonstrated that a 48-hour hypoxic challenge led to an unfolded protein response (UPR)-dependent depletion of $TBR2^+$ intermediate progenitors, which underwent an apparently precocious developmental transition to $CTIP2^+$ neurons [82]. Although we observed minimal induction of transcriptional markers of UPR and found only modest changes in the overall abundance of intermediate progenitor cells, our results are consistent with these findings, and suggest that the effects of hypoxia on intermediate progenitor cell development are visible even after a shorter exposure period. It is also possible that a sustained 48-hour shift from 21% to <1% oxygen induces a stronger effect with greater dependence on the UPR than our paradigm, which includes a period of adaptation to physiologic oxygen and a shorter hypoxic treatment. In either case, our data suggest that intermediate progenitor cells are especially labile in the face of fluctuating environmental oxygen, and may play an outsized role in linking transient oxygen stress to brain phenotypes [48,82].

We characterized gene regulatory variation in the context of normoxia, hypoxia, and hyperoxia. Though acute hypoxia-induced brain injury is relatively rare, transient fluctuations in brain oxygen availability are common, suggesting that the gene regulatory effects in this study may be pervasive in the population. For example, sleep apnea, in which repeated episodes of oxygen desaturation and restoration conspire to produce persistent oxidative stress, is estimated to affect nearly a billion people worldwide [83]. Recent studies using *in vivo* oxygen biosensors have also observed regions of local tissue hypoxia in rodent brains, both at rest and during demanding tasks [84,85]. While the significance of these minute-to-minute environmental fluctuations are not yet clear, their existence raises the possibility that hypoxia-evoked transcriptional changes may be ongoing features of the brain under normal conditions. Our results imply that these conditions elicit a host of gene expression changes with varying consequences across the population, and that those differences may in turn affect complex brain-related traits.

Our study focused on just three experimental conditions. By extending the topic modeling framework to a wider range of treatments, future studies could determine how many of the dynamic eQTLs we discovered can also be identified in the presence of other *in vitro* stressors. Recent technical advances, including supplementing organoids with non-neuronal cell types [86] and *in vivo* implantation [87–89], promise to dramatically expand the scope of disease-relevant interactions that can be captured in brain organoids and further extend the approach employed here. We expect that future studies of regulatory variation in these contexts will help prioritize targets for *in vivo* experimental manipulation.

Methods

Stem cell culture and organoid formation

We generated brain organoids using 21 iPSC lines (12 male, 9 female) that belong to an extensively characterized panel of iPSCs derived from Yoruba individuals from Ibadan, Nigeria (YRI) [51]. Stem cells were maintained on Matrigel-coated plates and fed with StemFlex media (Gibco)

supplemented with penicillin and streptomycin. Cells were passaged at least twice before organoid formation using 0.5 mM EDTA in PBS and seeded on new plates in the presence of CEPT [90].

Organoids were formed using a protocol modified from published methods [81,91–93]. Cells were dissociated using 0.5 mM EDTA in PBS and passed through a 40 µm filter, then aggregated by centrifugation in 96-well ultralow attachment round-bottom plates (Nunclon), with 10,000 cells per well in 100 µL of StemFlex medium with penicillin/streptomycin, 5 µM XAV, and CEPT. After 16-hour overnight incubation, medium was replaced with E6 medium supplemented with 100 nM LDN193189 (Cayman), 5 µM XAV939 (Cayman), 10 µM SB431542 (Cayman), 1X MEM non-essential amino acids (Gibco), and penicillin/streptomycin. Cell aggregates were fed with this medium every other day for seven days; XAV939 was removed from the medium after the fifth day. Aggregates were then fed with DMEM/F12 (Gibco) supplemented with N2 (1%, R&D Systems, AR009), Glutamax (1%, Gibco), chemically-defined lipid concentrate (1%, Gibco), heparin (1 µg/mL, Sigma), and penicillin/streptomycin every other day for four days. Organoids were then embedded in Matrigel droplets and transferred to ultralow attachment six-well plates (Nunclon) in 1:1 DMEM/F12:Neurobasal medium (Gibco) with chemically-defined lipid concentrate (1%), N2 supplement (0.5%), MEM NEAA (0.5%), Glutamax (1%), beta-mercaptoethanol, N21 without vitamin A (1%, R&D Systems AR012), insulin (2 µg/mL, Gibco), and penicillin/streptomycin. Organoids received this medium every other day for seven days, transferring to an orbital shaker on the fifth day (16 days after formation). After this point, the N21 supplement was replaced with N21 with vitamin A (1%, R&D Systems AR008) and organoids were fed three times per week. After three weeks in maintenance culture, organoids were gradually transitioned to BrainPhys-based medium, in which DMEM/F12/Neurobasal base medium was replaced with BrainPhys medium (StemCell Technologies). BrainPhys-based medium was introduced in 25% increments into the DMEM/F12/Neurobasal base medium over the course of four feedings. BrainPhys medium was originally optimized for monolayer culture[94] and contains 2.5 mM glucose, a little more than 10% of the concentration in a 1:1 mixture of DMEM/F12:Neurobasal and similar to or lower than human cerebrospinal fluid. The glucose concentration in our BrainPhys-based medium was supplemented to 10 mM (ThermoFisher, A2494001), just under half the concentration of DMEM/F12/Neurobasal-based medium. Organoids were maintained for four additional weeks in BrainPhys-based medium before sample collection for a total of eight weeks of maturation.

Low- and high-oxygen treatment

Organoids were collected in two batches. One week prior to sample collection, organoids were adapted to 10% oxygen (5% CO_2, nitrogen balance) in a HeraCell 150i incubator (ThermoFisher). During this period, medium was equilibrated to 10% oxygen prior to feeding, and organoids were fed 24 hours before oxygen stress treatment. At the start of the experiment, plates of organoids (6-8 organoids per iPSC line per condition) were transferred to incubators maintained at 1% oxygen (5% CO_2, nitrogen balance) or room oxygen (5% CO_2) or left at control conditions. Oxygen concentrations were verified with a probe-based oxygen meter (Apogee Instruments, MO-200), and rapid equilibration of cell culture medium to ambient oxygen levels was confirmed in separate pilot experiments using a PreSens Fibox3 dissolved oxygen measurement device. After 24 hours, organoids were collected for single-cell dissociation.

Single-cell RNA-sequencing sample preparation and processing

Organoids were processed using a combination of enzymatic and mechanical dissociation. Organoid medium was replaced with 1 mL papain solution (20 U/mL in EBSS, Worthington LK003150) with DNase I (100 U/mL, Worthington) supplemented with actinomycin D (5 µg/mL, Sigma A9415) and TTX (1 µM, Tocris 1069) and organoids were rapidly sheared with a pair of needles. Enzymatic digestion proceeded in the incubator, with continuous shaking, for 30 minutes. Organoids were pipetted twice with a 7-8 mm fire-polished Pasteur pipet, then returned to the incubator for an additional 10 minutes of enzymatic digestion. Samples were gently triturated four times each with fire-polished Pasteur pipets of decreasing widths (8, 6, and 3 mm) and heavy debris was allowed to settle. Samples were transferred to tubes with 2 mL inhibitor solution (3.75 mg/mL ovomucoid, 3.75

mg/mL albumin, 100 U/mL DNaseI, Worthington LK003150) and spun for 5 minutes at 200 g. Pellets were resuspended in cold Neurobasal medium with 0.5% BSA and actinomycin D and counted using a Countess II automated cell counter (Thermo) with Trypan blue. Cells from different individuals were pooled to equal concentrations, yielding three combined samples (control, low-oxygen, high-oxygen), spun down, resuspended in cold Neurobasal medium with actinomycin D, filtered with a 40 µm filter (Flowmi), and counted using a hemacytometer. Samples were loaded onto a 10x HT chip (10x Genomics) for single-cell encapsulation according to the manufacturer's instructions, targeting approximately 3,000 cells per individual per treatment condition. Sequencing libraries were prepared using the 10x Genomics 3' HT kit v3.1, according to the manufacturer's instructions, in a single batch, and libraries were sequenced according to 10x Genomics specifications, targeting a minimum of 20,000 reads per cell, on an Illumina NovaSeq 6000 instrument at the University of Chicago Genomics Core Facility (RRID:SCR_019196).

Single-cell RNA-sequencing data processing and annotation

Sequencing data were processed using the *cellranger* pipeline (v7.0.0) for read alignment (GRCh38) and cell detection. Samples were demultiplexed using *Vireo* [95] with imputed genotype information from the HapMap Project and 1000 Genomes Project, and droplets assigned to multiple individuals or with low-confidence assignments (singlet probability <0.95) were excluded. All subsequent cell filtering and annotation was performed using *Seurat* (v4.4.0) [96]. Cells were further filtered to exclude those with greater than 10% mitochondrial read content, fewer than 2,500 UMIs, or more than 20,000 UMIs, resulting in 170,841 retained cells (control = 52,671; hypoxia=57,788; hyperoxia=60,382). Data were normalized using *SCTransform* and integrated across batch and individual using *Harmony* [97] to minimize inter-individual differences in cell type annotation. All subsequent analyses made use of UMI counts, rather than transformed or fitted expression values.

Cells were annotated using a combination of reference mapping and clustering. First, cells were mapped to two published fetal single-cell datasets [52,53] using the *MapQuery* function in *Seurat*, excluding cell types absent in our organoids (microglia, endothelium, pericytes, erythrocytes), to obtain initial annotations for each cell. While most organoid cell types exhibited reasonably high concordance with fetal cell types, certain early and transitional cells could not be unambiguously annotated using the fetal reference data. To retain the information provided by these cells, which may be particularly valuable in the context of our *in vitro* experimental framework, a secondary unsupervised clustering approach was used. Dimensionality reduction and clustering were performed using *Seurat*, excluding cell cycle genes (*cc.genes* in *Seurat*) from the variable feature set to avoid spuriously co-clustering dividing radial glia and intermediate progenitor cells. A high clustering resolution was selected which produced more clusters than the fetal references and beyond which further increases did not yield interpretable changes in clusters (resolution 0.6). Clusters were then annotated based on the consensus of the fetal reference assignments of their constituent cells, or, in the case of discrepancy, additional marker gene expression, resulting in 20 cell type classes, including both "principal" cell types of the developing cerebral cortex and subtypes of neurons with regional or neuropeptide expression signatures. As fine cell type classification risks insufficient cell numbers in each group for some downstream analyses, a secondary, coarser set of annotations was created by grouping similar cell types (e.g., different inhibitory neuron subtypes) into 10 coarser classes (**Figure S1d**).

Changes in cell type abundance in response to oxygen manipulation were assessed using *propeller* [54]. Linear mixed models were estimated for both fine- and coarse-level annotations, using the treatment condition as a predictor and the parental iPSC line as a blocking variable. To further characterize sources of variation in cell type composition, additional experimental factors (collection batch, sex, iPSC passage number), were included in the model, although we note that only two iPSC lines allow direct comparisons across batches by repeated measures.

Differential expression analysis

To identify genes differentially expressed between treatment conditions, we relied on well-established methods for analyzing bulk RNA-sequencing data. Single-cell transcriptomes were summed to pseudobulk samples, each of which corresponded to one combination of individual, treatment condition, cell type, and collection batch. Oligodendrocytes and midbrain dopaminergic neurons excluded from analysis for lack of sufficient sample sizes.

Before fitting expression models, principal component analysis was used to identify important covariates contributing to gene expression variation. Sample variation was strongly driven by the number of cells contributing to a pseudobulk sample up to 10 cells/pseudobulk sample, with a weaker effect persisting up to 20 cells/pseudobulk sample. For differential expression testing, pseudobulk samples derived from fewer than 20 cells were excluded. Pseudobulk data were TMM-normalized and genes were filtered using the *filterByExpr* function in the *edgeR* package, using treatment condition as the primary comparison group. A separate linear mixed model was estimated for each cell type using *dream* [55], with treatment condition modeled as a fixed effect and batch and parental iPSC line as random effects.

For assessing the contribution of stress-responsive cells to differential expression results, we re-ran our analysis on two datasets. In the first, we removed stress-annotated cells from each cell type before running differential expression analysis (see below). As removing cells will decrease power to detect differential expression, we generated a second dataset in which we randomly removed an equivalent number of cells of each cell type as in our stress-censored data. We compared the ratio of differentially expressed genes in the two datasets in each cell type as a measure of the transcriptional response driven by cells identified as stressed.

Accurately assessing patterns of gene regulation shared across different cell types and contexts is complicated by incomplete power. In order to characterize patterns of sharing across different cell types and treatments, we used the *mashr* package [56] to estimate posterior effect sizes and significance, with the *udr* package used in place of the default extreme deconvolution algorithm [https://stephenslab.github.io/udr/index.html]. Genes were considered significantly differentially expressed with a posterior local false sign rate (lfsr) less than 0.05, and differential expression effects were considered shared if their posterior log fold-change estimates were within a factor of 2.5 of each other.

Enrichment analysis of DE genes

Differentially expressed genes were analyzed for enrichment of functionally defined categories using the *fgsea* package [98]. For each differential expression posterior mean and standard deviation estimate obtained from *mash*, a t-statistic was calculated and used as the ranking statistic for fgsea. The Hallmark gene sets [99] were obtained from MSigDB and used as the test set of pathways for all cell types and treatment comparisons.

Stressed cell identification

Cells were classified as stressed by adapting the *Gruffi* framework [61], which scores local neighborhoods of cells using positive- and negative-selection gene lists. The default *Gruffi* gene lists include gene ontology terms for glycolysis and endoplasmic reticulum stress. The ER stress score did not correlate with hypoxic treatment in our data, and neither score correlated with high-oxygen exposure. As an alternative, custom gene lists were identified by *mash* as being upregulated by treatment across all fine-classified cell types (minimum two-fold change for low-oxygen treatment, minimum 1.5-fold change for high-oxygen treatment), with similar responsiveness to treatment across cell types (maximum log fold-change no more than 5 times the median log fold-change), yielding a hypoxia treatment score based on 66 genes and a hyperoxia treatment score based on 7 non-overlapping genes (**Table S3**). These genes all have known roles in stress response, redox handling, or the HIF pathway. After cell neighborhood scoring, classification was performed using *Gruffi*, using the custom gene lists as positive selection features and the default negative selection

(gliogenesis-related genes) gene list. Cells were classified as hypoxia-responsive, hyperoxia-responsive, or as double-responsive, meaning they were classified by *Gruffi* as "stressed" using both gene lists. Only 223 cells were characterized as "double-responsive," all of which were annotated as VLMC. Sensitivity to treatment was calculated as the fractional change in the proportion of any cell type classified as responsive compared to the normoxia condition.

Immunofluorescent labeling and imaging

Organoids were washed with cold PBS and fixed with 4% paraformaldehyde (Electron Microscopy Sciences) in PBS at 4˚C for 45 minutes. Organoids were then washed three times with cold PBS and cryoprotected overnight in a 30% sucrose solution before being snap frozen in OCT (Fisher). Serial cryosections (14 µm) were collected in replicate slide sets spanning the thickness of the organoid. Sections were washed with PBS and blocked with 10% NDS (Jackson) and 0.3% Triton X-100 (Sigma) in PBS for one hour at room temperature. Antibodies were diluted as follows in PBS with 2% NDS and 0.1% Triton X-100 for staining overnight at 4˚C: HOPX (rabbit, 1:500, Proteintech, RRID AB_10693525), S100B (guinea pig, 1:500, Synaptic Systems, RRID AB_2620025), MKI67 (mouse, 1:500, Cell Signaling RRID AB_2797703), RELN (mouse, 3 µg/mL, DSHB RRID AB_1157892), GABA (rabbit, 1:500, GeneTex RRID AB_11173015), EOMES (rabbit, 1:500, GeneTex RRID AB_2887210), BCL11B (rat, 1:200, BioLegend RRID AB_10896795), SATB2 (mouse, 1:100, Fitzgerald AB_10809039), SOX2 (rabbit, 1:500, Synaptic Systems RRID AB_2620099), NES (mouse, 1:500, Santa Cruz RRID AB_1126569), GFAP (mouse, 3 µg/mL, DSHB N206A/8). Sections were washed four times with PBS-T (PBS with 0.05% Tween-20) and once with PBS, then incubated for two hours at room temperature with donkey secondary antibodies diluted in PBS with 2% NDS and 0.1% Triton X-100 as follows: anti-rabbit Alexa Fluor 488 (1:500, Invitrogen, RRID AB_141607), anti-guinea pig Alexa Fluor 647 (1:300, Jackson, RRID AB_2340476), anti-mouse Cy3 (1:300, Jackson, RRID AB_2340813), anti-rat Alexa Fluor 647 (1:300, Jackson, RRID AB_2340694), anti-mouse Alexa Fluor 647 (1:300, Jackson, RRID AB_2340862). Sections were washed four times in PBS-T, rinsed with water, and mounted with Fluoromount G with DAPI (Invitrogen). Slides were imaged on an Olympus VS200 Research Slide Scanner with a Hamamatsu ORca-Fusion Camera at the University of Chicago Integrated Light Microscopy Core facility, using the DAPI channel for focal mapping.

Image analysis

For each series of organoid cryosections, the largest section was considered to be the most medial and was retained for further analysis. Image segmentation and intensity measurements were performed using the *QuPath* (v0.4.3) software package with the *Stardist* extension [100,101]. The perimeter of each section was defined using a custom pixel classifier. Cells were detected using the *Stardist* fluorescence cell detection script (dsb2018_heavy_augment.pb), with detection threshold and resolution (*pixelSize*) parameters changed (from default 0.5 to 0.3) to better suit our images. For each identified nucleus, we obtained mean fluorescence intensities and the linear distance to the nearest section edge. Cells were classified as positive for each antibody marker using a per-section threshold (1-2 standard deviations above the mean across all nuclei within the section) determined for each antibody channel. Cell types were defined conservatively from antibody markers as follows: "dividing progenitors" were defined as $MKI67^+/S100B^-/HOPX^-$; "radial glia" were defined as $HOPX^+/S100B^-$, $MKI67^+/S100B^-/HOPX^+$, or $SOX2^+/S100B^+/NES^-$; "Cajal-Retzius cells" were defined as $RELN^+/GABA^-/BCL11B^-$; "intermediate progenitors" were defined as $EOMES^+/SATB2^-/BCL11B^-$; "immature excitatory neurons" were defined as $BCL11B^+/SATB2^-$; "mature excitatory neurons" were defined as $SATB2^+$; "inhibitory neurons" were defined as $GABA^+$ (including $GABA^+/RELN^+$ and $GABA^+/BCL11B^+$); "glia" were defined as $S100B^+/HOPX^-/MKI67^-$, $S100B^+/SOX2^+/NES^+$, or $GFAP^+$, consistent with marker combinations seen in our transcriptomic dataset. Note that these markers do not fully label all cells within a given cell type, and do not collectively cover all cell types observed by single-cell RNA-seq, but instead were chosen to localize identifiable groups of cells.

Topic modeling

Topic modeling offers an alternative to fixed-category classification of cell states, allowing for cells to be described quantitatively by multiple gene expression programs. To alleviate the computational burden of topic model estimation and downstream analysis, single-cell data were first aggregated into 10,707 "pseudocells" by first clustering at high resolution (resolution=20) and then splitting each cluster of related cells by parental cell line and treatment condition. The *fastTopics* package [102,103] was used to fit models with a range of topics (k=10-40), and the most parsimonious model that still retained a clear hypoxia-associated topic was selected. Models were estimated by Poisson non-negative matrix factorization (*fit_poisson_nmf*) of the pseudocell count data using 400 expectation-maximization steps, followed by 200 stochastic coordinate descent steps. A multinomial topic model was obtained using the *poisson2multinom* command. Individual topics were analyzed by grade-of-membership differential expression analysis [104], comparing topic-specific DE results to cell type- or treatment-specific marker genes.

Cis eQTL analysis

Cis eQTLs were identified separately for each combination of cell type and oxygen treatment condition using methods originally developed for bulk RNA-seq analysis. We obtained pseudobulk expression measurements by summing UMI counts for all protein-coding genes across cells grouped by parental iPSC line, treatment, and cell type, excluding pseudobulk samples derived from fewer than 20 cells. Cell types present in fewer than 7 individuals after pseudobulk filtering were excluded from subsequent analysis. Samples for each combination of cell type and oxygen exposure condition were TMM-normalized and expressed as log CPM values using the *edgeR* package [105]. Genes were filtered using the *filterByExpr* function in the *edgeR* package, with parameters min.count.cpm=6, min.prop.expr=0.5, and min.total.count=30, and the bottom quartile of genes ranked by standard deviation was omitted. Expression values were centered and scaled across individuals for each gene and, for each gene, rank-normalized across individuals [106]. QTL testing was performed using *MatrixEQTL* [107]. Genotype data were filtered to include variants with minor allele frequencies greater than 0.1 and Hardy-Weinberg equilibrium p-values greater than 10^{-6} using *vcftools*, and all variants within 50 kb of a gene's transcription start site were tested for association. Gene expression principal components, obtained using the *prcomp* function in R, were used as covariates. The number of gene expression principal component covariates was chosen for each cell type and treatment so as to explain more variance in our data than in a random permutation of the data [108].

Most genetic effects on gene expression are expected to be shared across conditions. To increase our ability to detect subtle eQTL effects, *mash* was used to compare the strongest variant-gene associations across treatment conditions independently within each cell type. Note that this approach does not allow us to make rigorous statements about sharing across different cell types, but rather across treatment conditions within a single cell type. *MatrixEQTL* output was reformatted, and input data structures were created using the *fastqtl2mash* tool [56]. Because samples from different treatment conditions derive from the same parental cell lines, we the correlation structure was first estimated using *mashr*'s expectation-maximization tool. Posterior eQTL effects were considered shared across two (or more) conditions if the variant-gene pair was significant (i.e., local false sign rate < 0.05) in at least one of the conditions and the posterior effect size estimates differed by a factor of less than 2.5. Conversely, eQTL effects were considered oxygen-responsive if they were not shared in at least one oxygen condition.

Topic-interacting cis eQTLs

Cis eQTLs that interact with cellular context were identified using *CellRegMap* [66]. The cellular environment for each pseudocell was defined by the 15-topic model estimated using *fastTopics*. Genetic similarity among pseudocells was obtained from *Plink* [109], and normalized gene expression counts for each pseudocell were used as input for *CellRegMap*. Because of the substantial computational cost of a genome-wide scan for interaction effects, tests

were restricted to eGenes initially identified in the standard pseudobulk eQTL framework, testing SNPs with equal or stronger evidence of association as the *mash* lead SNP in any condition. Significant *CellRegMap* results were defined by applying a q-value threshold of 0.1 to the Bonferroni-corrected p-values.

Comparison to disease genes

Disease-associated genes and variants were obtained from various sources (see **Tables S5 and S6**). For results obtained from the GWAS Catalog [110], intergenic variants were assigned to the gene reported in the initial study or, when no gene was reported, to the nearest gene. Traits were filtered to include at least 15 associations and no more than 500 associations, and associations were further filtered to consider only genome-wide significant results ($p<5x10^{-8}$). Of the resulting 2989 traits, 402 were categorized as having neurological or psychiatric relevance and the remaining were considered to be "off-target" traits (**Table S6**). For gene-level analyses, we compared eGenes (genes with significant eQTL effects after *mash*) to trait-associated genes. For variant-level comparisons, we used the lead variant used by *mash*, which is the variant with the strongest association in any of the three treatment conditions used as input.

For comparisons with genes harboring rare variants, we obtained gene lists from the SCHEMA [111], SFARI (syndromic and category 1 genes) [79], Epi25 [112], BipEx [74], and Deciphering Developmental Disorders [113] projects. We filtered these gene lists using the measures of significance available for each dataset to obtain a list of 1,672 unique genes (**Table S5**).

For comparisons with GTEx eGenes, we combined the eGenes found in "Brain Cortex" and "Brain Frontal Cortex" tissue in the GTEx v8 data release. For wider comparisons to assess the novelty and tissue distribution of example eQTLs, we queried the OpenTargets Genetics [71,72] database and results from the CommonMind Consortium [73].

Data and code availability:

Sequencing data have been deposited in GEO through series accession code GSE273907. Code used to generate the results and figures in this publication are available on Github: https://github.com/bumans/organoid_oxygen_eqtl.

Acknowledgements:

We thank Natalia Gonzalez, Katherine Rhodes, and Bradley Wierbowski for manuscript comments and Josh Popp, Wenhe Lin, Peter Carbonetto, Benjamin Fair, and Yunqi Yang for technical advice. Jonathan Burnett and Olivia Allen assisted with cell culture and cryosectioning. Imaging was performed at the University of Chicago Integrated Light Microscopy Core (RRID: SCR_019197), and sequencing was performed by the University of Chicago Genomics Facility (RRID: SCR_019196). This work was supported by a grant from the National Institutes of Health (R35GM131726 to YG).

Data were generated as part of the CommonMind Consortium supported by funding from Takeda Pharmaceuticals Company Limited, F. Hoffmann-La Roche Ltd and NIH grants R01MH085542, R01MH093725, P50MH066392, P50MH080405, R01MH097276, RO1-MH-075916, P50M096891, P50MH084053S1, R37MH057881, AG02219, AG05138, MH06692, R01MH110921, R01MH109677, R01MH109897, U01MH103392, and contract HHSN271201300031C through IRP NIMH. Brain tissue for the study was obtained from the following brain bank collections: the Mount Sinai NIH Brain and Tissue Repository, the University of Pennsylvania Alzheimer's Disease Core Center, the University of Pittsburgh NeuroBioBank and Brain and Tissue Repositories, and the NIMH Human Brain Collection Core. CMC Leadership: Panos Roussos, Joseph Buxbaum, Andrew Chess, Schahram Akbarian, Vahram Haroutunian (Icahn School of Medicine at Mount Sinai), Bernie Devlin, David Lewis (University of Pittsburgh), Raquel Gur, Chang-Gyu Hahn (University of Pennsylvania), Enrico Domenici (University of

Trento), Mette A. Peters, Solveig Sieberts (Sage Bionetworks), Thomas Lehner, Stefano Marenco, Barbara K. Lipska (NIMH)

"The results published here are in part based on data obtained from the AD Knowledge Portal (https://adknowledgeportal.org). Study data were provided by the Rush Alzheimer's Disease Center, Rush University Medical Center, Chicago, where data collection was supported through funding by NIA grants P30AG10161, R01AG15819, R01AG17917, R01AG36836, R01AG48015, U01AG46152, the Illinois Department of Public Health (ROSMAP), and the Translational Genomics Research Institute (genomic). The Mayo Clinic Alzheimers Disease Genetic Studies, led by Dr. Nilufer Taner and Dr. Steven G. Younkin, Mayo Clinic, Jacksonville, FL where data collection was supported through funding by NIA grants P50 AG016574, R01 AG032990, U01 AG046139, R01 AG018023, U01 AG006576, U01 AG006786, R01 AG025711, R01 AG017216, R01 AG003949, NINDS grant R01 NS080820, CurePSP Foundation, and support from Mayo Foundation. Study data includes samples collected through the Sun Health Research Institute Brain and Body Donation Program of Sun City, Arizona. The Brain and Body Donation Program is supported by the National Institute of Neurological Disorders and Stroke (U24 NS072026 National Brain and Tissue Resource for Parkinsons Disease and Related Disorders), the National Institute on Aging (P30 AG19610 Arizona Alzheimers Disease Core Center), the Arizona Department of Health Services (contract 211002, Arizona Alzheimers Research Center), the Arizona Biomedical Research Commission (contracts 4001, 0011, 05-901 and 1001 to the Arizona Parkinson's Disease Consortium) and the Michael J. Fox Foundation for Parkinsons Research. And, the CommonMind Consortium supported by funding from Takeda Pharmaceuticals Company Limited, F. Hoffmann-La Roche Ltd and NIH grants R01MH085542, R01MH093725, P50MH066392, P50MH080405, R01MH097276, RO1-MH-075916, P50M096891, P50MH084053S1, R37MH057881, AG02219, AG05138, MH06692, R01MH110921, R01MH109677, R01MH109897, U01MH103392, and contract HHSN271201300031C through IRP NIMH. Brain tissue for the study was obtained from the following brain bank collections: the Mount Sinai NIH Brain and Tissue Repository, the University of Pennsylvania Alzheimer's Disease Core Center, the University of Pittsburgh NeuroBioBank and Brain and Tissue Repositories, and the NIMH Human Brain Collection Core. CMC Leadership: Panos Roussos, Joseph Buxbaum, Andrew Chess, Schahram Akbarian, Vahram Haroutunian (Icahn School of Medicine at Mount Sinai), Bernie Devlin, David Lewis (University of Pittsburgh), Raquel Gur, Chang-Gyu Hahn (University of Pennsylvania), Enrico Domenici (University of Trento), Mette A. Peters, Solveig Sieberts (Sage Bionetworks), Thomas Lehner, Stefano Marenco, Barbara K. Lipska (NIMH)"

The DDD study presents independent research commissioned by the Health Innovation Challenge Fund [grant number HICF-1009-003]. This study makes use of DECIPHER (http://www.deciphergenomics.org), which is funded by Wellcome [grant number WT223718/Z/21/Z]. See Nature PMID: 25533962 or www.ddduk.org/access.html for full acknowledgement.

References

1. Zhang H, Khan A, Rzhetsky A. Gene-environment interactions explain a substantial portion of variability of common neuropsychiatric disorders. Cell Rep Med. 2022;3. doi:10.1016/j.xcrm.2022.100736

2. Hollander JA, Cory-Slechta DA, Jacka FN, Szabo ST, Guilarte TR, Bilbo SD, et al. Beyond the looking glass: recent advances in understanding the impact of environmental exposures on neuropsychiatric disease. Neuropsychopharmacology. 2020;45: 1086–1096. doi:10.1038/s41386-020-0648-5

3. Seah C, Signer R, Deans M, Bader H, Rusielewicz T, Hicks EM, et al. Common genetic variation impacts stress response in the brain. bioRxiv; 2023. p. 2023.12.27.573459. doi:10.1101/2023.12.27.573459

4. Moyerbrailean GA, Richards AL, Kurtz D, Kalita CA, Davis GO, Harvey CT, et al. High-throughput allele-specific expression across 250 environmental conditions. Genome Res. 2016;26: 1627–1638. doi:10.1101/gr.209759.116

5. Nguyen TTL, Gao H, Liu D, Philips TJ, Ye Z, Lee J-H, et al. Glucocorticoids unmask silent non-coding genetic risk variants for common diseases. Nucleic Acids Res. 2022;50: 11635–11653. doi:10.1093/nar/gkac1045

6. Brooks JTS, Elvidge GP, Glenny L, Gleadle JM, Liu C, Ragoussis J, et al. Variations within oxygen-regulated gene expression in humans. J Appl Physiol. 2009;106: 212–220. doi:10.1152/japplphysiol.90578.2008

7. Ward MC, Banovich NE, Sarkar A, Stephens M, Gilad Y. Dynamic effects of genetic variation on gene expression revealed following hypoxic stress in cardiomyocytes. eLife. 2021;10. doi:10.7554/eLife.57345

8. Alasoo K, Rodrigues J, Mukhopadhyay S, Knights AJ, Mann AL, Kundu K, et al. Shared genetic effects on chromatin and gene expression indicate a role for enhancer priming in immune response. Nat Genet. 2018;50: 424–431. doi:10.1038/s41588-018-0046-7

9. Barreiro LB, Tailleux L, Pai AA, Gicquel B, Marioni JC, Gilad Y. Deciphering the genetic architecture of variation in the immune response to Mycobacterium tuberculosis infection. Proc Natl Acad Sci. 2012;109: 1204–1209. doi:10.1073/pnas.1115761109

10. Kim-Hellmuth S, Bechheim M, Pütz B, Mohammadi P, Nédélec Y, Giangreco N, et al. Genetic regulatory effects modified by immune activation contribute to autoimmune disease associations. Nat Commun. 2017;8: 266. doi:10.1038/s41467-017-00366-1

11. Lee MN, Ye C, Villani A-C, Raj T, Li W, Eisenhaure TM, et al. Common genetic variants modulate pathogen-sensing responses in human dendritic cells. Science. 2014;343: 1246980. doi:10.1126/science.1246980

12. Fairfax BP, Humburg P, Makino S, Naranbhai V, Wong D, Lau E, et al. Innate immune activity conditions the effect of regulatory variants upon monocyte gene expression. Science. 2014;343: 1246949. doi:10.1126/science.1246949

13. Randolph HE, Fiege JK, Thielen BK, Mickelson CK, Shiratori M, Barroso-Batista J, et al. Genetic ancestry effects on the response to viral infection are pervasive but cell type specific. Science. 2021;374: 1127–1133. doi:10.1126/science.abg0928

14. THE GTEX CONSORTIUM. The GTEx Consortium atlas of genetic regulatory effects across human tissues. Science. 2020;369: 1318–1330. doi:10.1126/science.aaz1776

15. Findley AS, Monziani A, Richards AL, Rhodes K, Ward MC, Kalita CA, et al. Functional dynamic genetic effects on gene regulation are specific to particular cell types and environmental conditions. eLife. 2021;10. doi:10.7554/eLife.67077

16. Umans BD, Battle A, Gilad Y. Where Are the Disease-Associated eQTLs? Trends Genet. 2021;37: 109–124. doi:10.1016/j.tig.2020.08.009

17. Walker RL, Ramaswami G, Hartl C, Mancuso N, Gandal MJ, de la Torre-Ubieta L, et al. Genetic Control of Expression and Splicing in Developing Human Brain Informs Disease Mechanisms. Cell. 2019;179: 750-771.e22. doi:10.1016/j.cell.2019.09.021

18. Emani PS, Liu JJ, Clarke D, Jensen M, Warrell J, Gupta C, et al. Single-cell genomics and regulatory networks for 388 human brains. Science. 2024;384: eadi5199. doi:10.1126/science.adi5199

19. Jerber J, Seaton DD, Cuomo ASE, Kumasaka N, Haldane J, Steer J, et al. Population-scale single-cell RNA-seq profiling across dopaminergic neuron differentiation. Nat Genet. 2021;53: 304–312. doi:10.1038/s41588-021-00801-6

20. Aygün N, Elwell AL, Liang D, Lafferty MJ, Cheek KE, Courtney KP, et al. Brain-trait-associated variants impact cell-type-specific gene regulation during neurogenesis. Am J Hum Genet. 2021;108: 1647–1668. doi:10.1016/j.ajhg.2021.07.011

21. Wen C, Margolis M, Dai R, Zhang P, Przytycki PF, Vo DD, et al. Cross-ancestry, cell-type-informed atlas of gene, isoform, and splicing regulation in the developing human brain. medRxiv. 2023; 2023.03.03.23286706. doi:10.1101/2023.03.03.23286706

22. Schumann G, Andreassen OA, Banaschewski T, Calhoun VD, Clinton N, Desrivieres S, et al. Addressing Global Environmental Challenges to Mental Health Using Population Neuroscience: A Review. JAMA Psychiatry. 2023;80: 1066–1074. doi:10.1001/jamapsychiatry.2023.2996

23. Cobley JN, Fiorello ML, Bailey DM. 13 reasons why the brain is susceptible to oxidative stress. Redox Biol. 2018;15: 490–503. doi:10.1016/j.redox.2018.01.008

24. Salmaso N, Jablonska B, Scafidi J, Vaccarino FM, Gallo V. Neurobiology of premature brain injury. Nat Neurosci. 2014;17: 341–346. doi:10.1038/nn.3604

25. Erickson G, Dobson NR, Hunt CE. Immature control of breathing and apnea of prematurity: the known and unknown. J Perinatol Off J Calif Perinat Assoc. 2021;41: 2111–2123. doi:10.1038/s41372-021-01010-z

26. Wehby GL. Living on higher ground reduces child neurodevelopment-evidence from South America. J Pediatr. 2013;162: 606-611.e1. doi:10.1016/j.jpeds.2012.09.011

27. Prabhakar NR, Peng Y-J, Nanduri J. Hypoxia-inducible factors and obstructive sleep apnea. J Clin Invest. 2020;130: 5042–5051. doi:10.1172/JCI137560

28. Lavie L. Oxidative stress in obstructive sleep apnea and intermittent hypoxia--revisited--the bad ugly and good: implications to the heart and brain. Sleep Med Rev. 2015;20: 27–45. doi:10.1016/j.smrv.2014.07.003

29. Giannopoulou I, Pagida MA, Briana DD, Panayotacopoulou MT. Perinatal hypoxia as a risk factor for psychopathology later in life: the role of dopamine and neurotrophins. Hormones. 2018;17: 25–32. doi:10.1007/s42000-018-0007-7

30. Cannon TD, van Erp TGM, Rosso IM, Huttunen M, Lönnqvist J, Pirkola T, et al. Fetal Hypoxia and Structural Brain Abnormalities in Schizophrenic Patients, Their Siblings, and Controls. Arch Gen Psychiatry. 2002;59: 35–41. doi:10.1001/archpsyc.59.1.35

31. Jackson ML, Howard ME, Barnes M. Cognition and daytime functioning in sleep-related breathing disorders. Prog Brain Res. 2011;190: 53–68. doi:10.1016/B978-0-444-53817-8.00003-7

32. Zacharias HU, Weihs A, Habes M, Wittfeld K, Frenzel S, Rashid T, et al. Association Between Obstructive Sleep Apnea and Brain White Matter Hyperintensities in a Population-Based Cohort in Germany. JAMA Netw Open. 2021;4: e2128225. doi:10.1001/jamanetworkopen.2021.28225

33. Kim H, Yun C-H, Thomas RJ, Lee SH, Seo HS, Cho ER, et al. Obstructive sleep apnea as a risk factor for cerebral white matter change in a middle-aged and older general population. Sleep. 2013;36: 709-715B. doi:10.5665/sleep.2632

34. Owen JE, BenediktsdÓttir B, Gislason T, Robinson SR. Neuropathological investigation of cell layer thickness and myelination in the hippocampus of people with obstructive sleep apnea. Sleep. 2019;42: zsy199. doi:10.1093/sleep/zsy199

35. Garcia A, Reljic T, Pogoda TK, Kenney K, Agyemang A, Troyanskaya M, et al. Obstructive Sleep Apnea Risk Is Associated with Cognitive Impairment after Controlling for Mild Traumatic Brain Injury History: A Chronic Effects of Neurotrauma Consortium Study. J Neurotrauma. 2020;37: 2517–2527. doi:10.1089/neu.2019.6916

36. Halbower AC, Degaonkar M, Barker PB, Earley CJ, Marcus CL, Smith PL, et al. Childhood obstructive sleep apnea associates with neuropsychological deficits and neuronal brain injury. PLoS Med. 2006;3: e301. doi:10.1371/journal.pmed.0030301

37. Thomas RJ, Rosen BR, Stern CE, Weiss JW, Kwong KK. Functional imaging of working memory in obstructive sleep-disordered breathing. J Appl Physiol. 2005;98: 2226–2234. doi:10.1152/japplphysiol.01225.2004

38. Daulatzai MA. Evidence of neurodegeneration in obstructive sleep apnea: Relationship between obstructive sleep apnea and cognitive dysfunction in the elderly. J Neurosci Res. 2015;93: 1778–1794. doi:10.1002/jnr.23634

39. Blesa J, Trigo-Damas I, Quiroga-Varela A, Jackson-Lewis VR. Oxidative stress and Parkinson's disease. Front Neuroanat. 2015;9: 91. doi:10.3389/fnana.2015.00091

40. Varçin M, Bentea E, Michotte Y, Sarre S. Oxidative stress in genetic mouse models of Parkinson's disease. Oxid Med Cell Longev. 2012;2012: 624925. doi:10.1155/2012/624925

41. Wan Y-W, Al-Ouran R, Mangleburg CG, Perumal TM, Lee TV, Allison K, et al. Meta-Analysis of the Alzheimer's Disease Human Brain Transcriptome and Functional Dissection in Mouse Models. Cell Rep. 2020;32: 107908. doi:10.1016/j.celrep.2020.107908

42. Ionescu-Tucker A, Cotman CW. Emerging roles of oxidative stress in brain aging and Alzheimer's disease. Neurobiol Aging. 2021;107: 86–95. doi:10.1016/j.neurobiolaging.2021.07.014

43. Dias V, Junn E, Mouradian MM. The role of oxidative stress in Parkinson's disease. J Park Dis. 2013;3: 461–491. doi:10.3233/JPD-130230

902 44. Lin MT, Beal MF. Mitochondrial dysfunction and oxidative stress in neurodegenerative
903 diseases. Nature. 2006;443: 787–795. doi:10.1038/nature05292

904 45. Luk KC. Oxidative stress and α-synuclein conspire in vulnerable neurons to promote
905 Parkinson's disease progression. J Clin Invest. 2019;129: 3530–3531.
906 doi:10.1172/JCI130351

907 46. Musgrove RE, Helwig M, Bae E-J, Aboutalebi H, Lee S-J, Ulusoy A, et al. Oxidative
908 stress in vagal neurons promotes parkinsonian pathology and intercellular α-synuclein
909 transfer. J Clin Invest. 2019;129: 3738–3753. doi:10.1172/JCI127330

910 47. Kwak M, Lim S, Kang E, Furmanski O, Song H, Ryu YK, et al. Effects of Neonatal
911 Hypoxic-Ischemic Injury and Hypothermic Neuroprotection on Neural Progenitor Cells in
912 the Mouse Hippocampus. Dev Neurosci. 2015;37: 428–439. doi:10.1159/000430862

913 48. Romanko MJ, Rothstein RP, Levison SW. Neural Stem Cells in the Subventricular Zone
914 are Resilient to Hypoxia/Ischemia whereas Progenitors are Vulnerable. J Cereb Blood
915 Flow Metab. 2004;24: 814–825. doi:10.1097/01.WCB.0000123906.17746.00

916 49. Ren S-Y, Xia Y, Yu B, Lei Q-J, Hou P-F, Guo S, et al. Growth hormone promotes myelin
917 repair after chronic hypoxia via triggering pericyte-dependent angiogenesis. Neuron.
918 2024;112: 2177-2196.e6. doi:10.1016/j.neuron.2024.03.026

919 50. Komitova M, Xenos D, Salmaso N, Tran KM, Brand T, Schwartz ML, et al. Hypoxia-
920 Induced Developmental Delays of Inhibitory Interneurons Are Reversed by
921 Environmental Enrichment in the Postnatal Mouse Forebrain. J Neurosci. 2013;33:
922 13375–13387. doi:10.1523/JNEUROSCI.5286-12.2013

923 51. Banovich NE, Li YI, Raj A, Ward MC, Greenside P, Calderon D, et al. Impact of
924 regulatory variation across human iPSCs and differentiated cells. Genome Res. 2018;28:
925 122–131. doi:10.1101/gr.224436.117

926 52. Trevino AE, Müller F, Andersen J, Sundaram L, Kathiria A, Shcherbina A, et al.
927 Chromatin and gene-regulatory dynamics of the developing human cerebral cortex at
928 single-cell resolution. Cell. 2021;184: 5053-5069.e23. doi:10.1016/j.cell.2021.07.039

929 53. Polioudakis D, de la Torre-Ubieta L, Langerman J, Elkins AG, Shi X, Stein JL, et al. A
930 Single-Cell Transcriptomic Atlas of Human Neocortical Development during Mid-
931 gestation. Neuron. 2019;103: 785-801.e8. doi:10.1016/j.neuron.2019.06.011

932 54. Phipson B, Sim CB, Porrello ER, Hewitt AW, Powell J, Oshlack A. propeller: testing for
933 differences in cell type proportions in single cell data. Bioinformatics. 2022;38: 4720–
934 4726. doi:10.1093/bioinformatics/btac582

935 55. Hoffman GE, Roussos P. Dream: powerful differential expression analysis for repeated
936 measures designs. Bioinformatics. 2021;37: 192–201. doi:10.1093/bioinformatics/btaa687

937 56. Urbut SM, Wang G, Carbonetto P, Stephens M. Flexible statistical methods for estimating
938 and testing effects in genomic studies with multiple conditions. Nat Genet. 2019;51: 187–
939 195. doi:10.1038/s41588-018-0268-8

940 57. Chi J-T, Wang Z, Nuyten DSA, Rodriguez EH, Schaner ME, Salim A, et al. Gene
941 Expression Programs in Response to Hypoxia: Cell Type Specificity and Prognostic

Significance in Human Cancers. PLOS Med. 2006;3: e47. doi:10.1371/journal.pmed.0030047

58. Chang AJ, Ortega FE, Riegler J, Madison DV, Krasnow MA. Oxygen regulation of breathing through an olfactory receptor activated by lactate. Nature. 2015;527: 240–244. doi:10.1038/nature15721

59. Cummins EP, Taylor CT. Hypoxia-responsive transcription factors. Pflüg Arch. 2005;450: 363–371. doi:10.1007/s00424-005-1413-7

60. Semenza GL. Hypoxia-inducible factors in physiology and medicine. Cell. 2012;148: 399–408. doi:10.1016/j.cell.2012.01.021

61. Vértesy Á, Eichmüller OL, Naas J, Novatchkova M, Esk C, Balmaña M, et al. Gruffi: an algorithm for computational removal of stressed cells from brain organoid transcriptomic datasets. EMBO J. 2022;41: e111118. doi:10.15252/embj.2022111118

62. Moore SA, Iulianella A. Development of the mammalian cortical hem and its derivatives: the choroid plexus, Cajal–Retzius cells and hippocampus. Open Biol. 2021;11: 210042. doi:10.1098/rsob.210042

63. Panousis NI, Garwany OE, Knights A, Rop JC, Kumasaka N, Imaz M, et al. Gene expression QTL mapping in stimulated iPSC-derived macrophages provides insights into common complex diseases. bioRxiv; 2023. p. 2023.05.29.542425. doi:10.1101/2023.05.29.542425

64. Natri HM, Azodi CBD, Peter L, Taylor CJ, Chugh S, Kendle R, et al. Cell type-specific and disease-associated eQTL in the human lung. bioRxiv; 2023. p. 2023.03.17.533161. doi:10.1101/2023.03.17.533161

65. Popp JM, Rhodes K, Jangi R, Li M, Barr K, Tayeb K, et al. Cell-type and dynamic state govern genetic regulation of gene expression in heterogeneous differentiating cultures. bioRxiv; 2024. p. 2024.05.02.592174. doi:10.1101/2024.05.02.592174

66. Cuomo ASE, Heinen T, Vagiaki D, Horta D, Marioni JC, Stegle O. CellRegMap: a statistical framework for mapping context□specific regulatory variants using scRNA□seq. Mol Syst Biol. 2022;18: e10663. doi:10.15252/msb.202110663

67. Cong Y, So V, Tijssen MAJ, Verbeek DS, Reggiori F, Mauthe M. WDR45, one gene associated with multiple neurodevelopmental disorders. Autophagy. 2021;17: 3908–3923. doi:10.1080/15548627.2021.1899669

68. Johansson E, Grassi ES, Pantazopoulou V, Tong B, Lindgren D, Berg TJ, et al. CD44 Interacts with HIF-2α to Modulate the Hypoxic Phenotype of Perinecrotic and Perivascular Glioma Cells. Cell Rep. 2017;20: 1641–1653. doi:10.1016/j.celrep.2017.07.049

69. Liang G, Li S, Du W, Ke Q, Cai J, Yang J. Hypoxia regulates CD44 expression via hypoxia-inducible factor-1α in human gastric cancer cells. Oncol Lett. 2017;13: 967–972. doi:10.3892/ol.2016.5473

70. Zhao B, Zhang J, Ibrahim JG, Luo T, Santelli RC, Li Y, et al. Large-scale GWAS reveals genetic architecture of brain white matter microstructure and genetic overlap with

cognitive and mental health traits (n = 17,706). Mol Psychiatry. 2021;26: 3943–3955. doi:10.1038/s41380-019-0569-z

71. Ghoussaini M, Mountjoy E, Carmona M, Peat G, Schmidt EM, Hercules A, et al. Open Targets Genetics: systematic identification of trait-associated genes using large-scale genetics and functional genomics. Nucleic Acids Res. 2021;49: D1311–D1320. doi:10.1093/nar/gkaa840

72. Mountjoy E, Schmidt EM, Carmona M, Schwartzentruber J, Peat G, Miranda A, et al. An open approach to systematically prioritize causal variants and genes at all published human GWAS trait-associated loci. Nat Genet. 2021;53: 1527–1533. doi:10.1038/s41588-021-00945-5

73. Sieberts SK, Perumal TM, Carrasquillo MM, Allen M, Reddy JS, Hoffman GE, et al. Large eQTL meta-analysis reveals differing patterns between cerebral cortical and cerebellar brain regions. Sci Data. 2020;7: 340–11. doi:10.1038/s41597-020-00642-8

74. Palmer DS, Howrigan DP, Chapman SB, Adolfsson R, Bass N, Blackwood D, et al. Exome sequencing in bipolar disorder identifies AKAP11 as a risk gene shared with schizophrenia. Nat Genet. 2022;54: 541–547. doi:10.1038/s41588-022-01034-x

75. Peyrot WJ, Price AL. Identifying loci with different allele frequencies among cases of eight psychiatric disorders using CC-GWAS. Nat Genet. 2021;53: 445–454. doi:10.1038/s41588-021-00787-1

76. Lee PH, Anttila V, Won H, Feng Y-CA, Rosenthal J, Zhu Z, et al. Genomic Relationships, Novel Loci, and Pleiotropic Mechanisms across Eight Psychiatric Disorders. Cell. 2019;179: 1469-1482.e11. doi:10.1016/j.cell.2019.11.020

77. Lam M, Hill WD, Trampush JW, Yu J, Knowles E, Davies G, et al. Pleiotropic Meta-Analysis of Cognition, Education, and Schizophrenia Differentiates Roles of Early Neurodevelopmental and Adult Synaptic Pathways. Am J Hum Genet. 2019;105: 334–350. doi:10.1016/j.ajhg.2019.06.012

78. Wu Y, Cao H, Baranova A, Huang H, Li S, Cai L, et al. Multi-trait analysis for genome-wide association study of five psychiatric disorders. Transl Psychiatry. 2020;10: 1–11. doi:10.1038/s41398-020-00902-6

79. Abrahams BS, Arking DE, Campbell DB, Mefford HC, Morrow EM, Weiss LA, et al. SFARI Gene 2.0: a community-driven knowledgebase for the autism spectrum disorders (ASDs). Mol Autism. 2013;4: 36. doi:10.1186/2040-2392-4-36

80. Nagel M, Watanabe K, Stringer S, Posthuma D, van der Sluis S. Item-level analyses reveal genetic heterogeneity in neuroticism. Nat Commun. 2018;9: 905. doi:10.1038/s41467-018-03242-8

81. Velasco S, Kedaigle AJ, Simmons SK, Nash A, Rocha M, Quadrato G, et al. Individual brain organoids reproducibly form cell diversity of the human cerebral cortex. Nature. 2019;570: 523–527. doi:10.1038/s41586-019-1289-x

82. Pa□ca AM, Park J-Y, Shin H-W, Qi Q, Revah O, Krasnoff R, et al. Human 3D cellular model of hypoxic brain injury of prematurity. Nat Med. 2019;25: 784–791. doi:10.1038/s41591-019-0436-0

83. Benjafield AV, Ayas NT, Eastwood PR, Heinzer R, Ip MSM, Morrell MJ, et al. Estimation of the global prevalence and burden of obstructive sleep apnoea: a literature-based analysis. Lancet Respir Med. 2019;7: 687–698. doi:10.1016/S2213-2600(19)30198-5

84. Butt UJ, Steixner-Kumar AA, Depp C, Sun T, Hassouna I, Wüstefeld L, et al. Hippocampal neurons respond to brain activity with functional hypoxia. Mol Psychiatry. 2021;26: 1790–1807. doi:10.1038/s41380-020-00988-w

85. Beinlich FRM, Asiminas A, Untiet V, Bojarowska Z, Plá V, Sigurdsson B, et al. Oxygen imaging of hypoxic pockets in the mouse cerebral cortex. Science. 2024;383: 1471–1478. doi:10.1126/science.adn1011

86. Schafer ST, Mansour AA, Schlachetzki JCM, Pena M, Ghassemzadeh S, Mitchell L, et al. An in vivo neuroimmune organoid model to study human microglia phenotypes. Cell. 2023;186: 2111-2126.e20. doi:10.1016/j.cell.2023.04.022

87. Pa□ca SP. Constructing human neural circuits in living systems by transplantation. Cell. 2024;187: 8–13. doi:10.1016/j.cell.2023.12.008

88. Revah O, Gore F, Kelley KW, Andersen J, Sakai N, Chen X, et al. Maturation and circuit integration of transplanted human cortical organoids. Nature. 2022;610: 319–326. doi:10.1038/s41586-022-05277-w

89. Mansour AA, Gonçalves JT, Bloyd CW, Li H, Fernandes S, Quang D, et al. An in vivo model of functional and vascularized human brain organoids. Nat Biotechnol. 2018;36: 432–441. doi:10.1038/nbt.4127

90. Chen Y, Tristan CA, Chen L, Jovanovic VM, Malley C, Chu P-H, et al. A versatile polypharmacology platform promotes cytoprotection and viability of human pluripotent and differentiated cells. Nat Methods. 2021;18: 528–541. doi:10.1038/s41592-021-01126-2

91. Cederquist GY, Asciolla JJ, Tchieu J, Walsh RM, Cornacchia D, Resh MD, et al. Specification of positional identity in forebrain organoids. Nat Biotechnol. 2019;37: 436–444. doi:10.1038/s41587-019-0085-3

92. Lancaster MA, Knoblich JA. Generation of cerebral organoids from human pluripotent stem cells. Nat Protoc. 2014;9: 2329–2340. doi:10.1038/nprot.2014.158

93. Yoon S-J, Elahi LS, Pa□ca AM, Marton RM, Gordon A, Revah O, et al. Reliability of human cortical organoid generation. Nat Methods. 2019;16: 75–78. doi:10.1038/s41592-018-0255-0

94. Bardy C, van den Hurk M, Eames T, Marchand C, Hernandez RV, Kellogg M, et al. Neuronal medium that supports basic synaptic functions and activity of human neurons in vitro. Proc Natl Acad Sci. 2015;112: E2725-34. doi:10.1073/pnas.1504393112

95. Huang Y, McCarthy DJ, Stegle O. Vireo: Bayesian demultiplexing of pooled single-cell RNA-seq data without genotype reference. Genome Biol. 2019;20: 273–12. doi:10.1186/s13059-019-1865-2

96. Hao Y, Hao S, Andersen-Nissen E, Mauck III WM, Zheng S, Butler A, et al. Integrated analysis of multimodal single-cell data. Cell. 2021; 1–45. doi:10.1016/j.cell.2021.04.048

97. Korsunsky I, Millard N, Fan J, Slowikowski K, Zhang F, Wei K, et al. Fast, sensitive and accurate integration of single-cell data with Harmony. Nat Methods. 2019;16: 1289–1296. doi:10.1038/s41592-019-0619-0

98. Korotkevich G, Sukhov V, Budin N, Shpak B, Artyomov MN, Sergushichev A. Fast gene set enrichment analysis. bioRxiv; 2021. p. 060012. doi:10.1101/060012

99. Liberzon A, Birger C, Thorvaldsdóttir H, Ghandi M, Mesirov JP, Tamayo P. The Molecular Signatures Database (MSigDB) hallmark gene set collection. Cell Syst. 2015;1: 417–425. doi:10.1016/j.cels.2015.12.004

100. Schmidt U, Weigert M, Broaddus C, Myers G. Cell Detection with Star-convex Polygons. arXiv.org. 2018. pp. 265–273. doi:https://doi.org/10.48550/arXiv.1806.03535

101. Bankhead P, Loughrey MB, Fernández JA, Dombrowski Y, McArt DG, Dunne PD, et al. QuPath: Open source software for digital pathology image analysis. Sci Rep. 2017;7: 16878. doi:10.1038/s41598-017-17204-5

102. Dey KK, Hsiao CJ, Stephens M. Visualizing the structure of RNA-seq expression data using grade of membership models. PLOS Genet. 2017;13: e1006599. doi:10.1371/journal.pgen.1006599

103. Carbonetto P, Sarkar A, Wang Z, Stephens M. Non-negative matrix factorization algorithms greatly improve topic model fits. arXiv; 2022. doi:10.48550/arXiv.2105.13440

104. Carbonetto P, Luo K, Sarkar A, Hung A, Tayeb K, Pott S, et al. GoM DE: interpreting structure in sequence count data with differential expression analysis allowing for grades of membership. Genome Biol. 2023;24: 236. doi:10.1186/s13059-023-03067-9

105. Robinson MD, McCarthy DJ, Smyth GK. edgeR: a Bioconductor package for differential expression analysis of digital gene expression data. Bioinformatics. 2010;26: 139–140. doi:10.1093/bioinformatics/btp616

106. Degner JF, Pai AA, Pique-Regi R, Veyrieras J-B, Gaffney DJ, Pickrell JK, et al. DNase I sensitivity QTLs are a major determinant of human expression variation. Nature. 2012;482: 390–394. doi:10.1038/nature10808

107. Shabalin AA. Matrix eQTL: ultra fast eQTL analysis via large matrix operations. Bioinformatics. 2012;28: 1353–1358. doi:10.1093/bioinformatics/bts163

108. Kumasaka N, Knights AJ, Gaffney DJ. Fine-mapping cellular QTLs with RASQUAL and ATAC-seq. Nat Genet. 2016;48: 206–213. doi:10.1038/ng.3467

109. Chang CC, Chow CC, Tellier LC, Vattikuti S, Purcell SM, Lee JJ. Second-generation PLINK: rising to the challenge of larger and richer datasets. GigaScience. 2015;4: s13742-015-0047–8. doi:10.1186/s13742-015-0047-8

110. Sollis E, Mosaku A, Abid A, Buniello A, Cerezo M, Gil L, et al. The NHGRI-EBI GWAS Catalog: knowledgebase and deposition resource. Nucleic Acids Res. 2023;51: D977–D985. doi:10.1093/nar/gkac1010

111. Singh T, Poterba T, Curtis D, Akil H, Al Eissa M, Barchas JD, et al. Rare coding variants in 10 genes confer substantial risk for schizophrenia. Nature. 2022;604: 509–516. doi:10.1038/s41586-022-04556-w

112. Collaborative E, Chen S, Neale BM, Berkovic SF. Shared and distinct ultra-rare genetic risk for diverse epilepsies: A whole-exome sequencing study of 54,423 individuals across multiple genetic ancestries. medRxiv; 2023. p. 2023.02.22.23286310. doi:10.1101/2023.02.22.23286310

113. Fitzgerald TW, Gerety SS, Jones WD, van Kogelenberg M, King DA, McRae J, et al. Large-scale discovery of novel genetic causes of developmental disorders. Nature. 2015;519: 223–228. doi:10.1038/nature14135

Figure Legends

Figure 1. A panel of brain organoids yields diverse cell types across individuals. **(a)** Workflow of data collection. Brain organoids were first differentiated (see Methods) and adapted to physiological oxygen before 24-hour exposure to high, low, or control oxygen levels. Data shown in this figure are taken from the 10% "normoxia" condition. **(b)** UMAP representation of organoid single-cell transcriptomes highlighting principal cell types obtained across all individuals in our iPSC panel in the normoxia condition. **(c)** Proportion of cells from each parental cell line by annotation, with colors corresponding to the UMAP shown in (b).

Figure 2. Transcriptional responses of brain organoids to oxygen changes. **(a)** Fraction of shared differential expression effects between cell types and conditions. Sharing was assessed from MASH posterior estimates of significance and effect sizes (see Methods and Figure S2). **(b)** Enrichment of gene annotations among differentially expressed genes across cell types and conditions. Annotations are taken from the MSigDB Hallmark gene sets, with enrichments calculated by *fgsea*. **(c)** Fractional change in hypoxia-stressed fraction of each cell type after hypoxia exposure (coarse cell classification). Cells were classified as hypoxia-stressed or hyperoxia-stressed by *Gruffi* using a gene set derived from treatment responses shared across all cell types. See also Figure S4. **(d)** Distribution of cell distances to organoid perimeters measured after immunofluorescent labeling. "Unlabeled" measurements are derived from DAPI-labeled nuclei with no immunofluorescent label. Black dots represent sample means. Note that "Dividing Cells" encompass both dividing radial glia and dividing intermediate progenitors. **(e)** Average topic loading for each cell type and treatment condition. Topic 7 tracks hypoxia exposure, while other topics reflect processes found in one or several cell types.

Figure 3. Discovery of treatment context-specific eQTL effects across cell types. **(a)** Number of eGenes identified in each cell type, classified as "standard" (blue) or oxygen-responsive (red) according to contexts in which effect sizes differ by less than 2.5-fold. For each category of oxygen-responsive eGenes, shared effects are indicated by orange lines and the condition with a uniquely different eQTL effect is bolded (N = normoxia, lo = hypoxia, hi = hyperoxia). Total eQTLs of each category are indicated by stars (right axis). **(b)** Number of eGenes identified in each cell type, classified by sharing across oxygen treatment conditions and detection in normoxia condition. Light and dark shades of red and blue categories, respectively, sum to the blue and red categories shown in (a). **(c)** Fraction of eGenes identified in this study that are classified as eGenes in GTEx cerebral cortex tissues (see Methods). Treatment context-specific eGenes that were not detected in control conditions were less likely to be found in GTEx ($p=0.0067$, one-sided paired Wilcoxon test of oxygen-insensitive category against oxygen-responsive/undetected in normoxia category).

Figure 4. Organoid eQTLs can help interpret human disease genetics. **(a)** Example topic-interacting eQTLs. *ABCA1* expression is correlated with the inferred cell environment, as defined by linear combinations of topics, and this effect is largely driven by cortical hem and glial progenitor topic 15 in a genotype-dependent manner. The *WDR45B* eQTL effect is largely explained by hypoxia-associated topic 7. Each point corresponds to a single pseudocell used for CellRegMap topic interaction QTL mapping. **(b)** Number of eGenes in each cell type which are the nearest gene to a genome-wide significant GWAS finding among 402 brain-related traits. **(c)** Example of a cell type- and treatment-specific regulatory association matching a significant GWAS variant. **(d)** Number of eGenes in each cell type and discovery condition for which rare loss-of-function alleles have been associated with disease (see Methods).

Figure S1. Characterization of organoid cell type composition. **(a)** Marker gene expression in each cell type annotated in Figure 1. **(b)** Organoids maintained at atmospheric (21%) or

physiological (10%) oxygen for 1 week prior to collection show similar patterns of cell type composition. **(c)** Two samples were collected twice from distinct organoid formation batches. Although principal cell types are present in similar proportions, batches differ in the abundance of inhibitory neurons (gray), VLMC (lime green), mature excitatory neurons, and unclassified other neurons (blue). **(d)** Correspondence between "fine" and "coarse" classification of cell types. **(e)** Number of individuals retained per cell type after pseudobulk filtering, and number of cell types retained per individual, in the normoxia condition (representative of all sample collection conditions). Dashed lines indicate medians.

Figure S2. Differential expression after oxygen manipulation. **(a)** Composition of organoid samples across individuals and treatment conditions. Note that control condition data are identical to those shown in Figure 1. **(b)** Shared fraction across cell types and conditions for genes with expression changes >1.5-fold. **(c)** Proportion of tested genes in each cell type that were differentially expressed (FDR<0.05, light colors; FDR<0.05 and fold-change>1.5, dark colors). The number of genes tested in each comparison is plotted as a line (right axis). **(d)** Differential expression results for coarsely classified cells, as shown in (c). **(e)** Proportion of differential expression effects (FDR<0.05, left; FDR<0.05 and fold-change>1.5, right) shared between cell types and treatment conditions in coarsely classified cells, analogous to Figures 2a and S2b.

Figure S3. Cell abundance explains some, but not all, differences in differential expression results between cell types. **(a)** Total number of differentially expressed genes (FDR<0.05) in each cell type increases with cell type abundance, and corresponding number of individuals in differential expression comparison. **(b)** The effect shown in (a) is not driven by differences in transcriptome size or numbers of genes tested across cell types. Note that even among cell types of similar abundance, differential expression detection rate varies by almost twofold. **(c)** Results as shown in (a), excluding small differential expression effects (<1.5-fold change). Note that excess DE genes discovered in abundant cell types largely show small effect sizes. **(d)** Volcano plots of grade-of-membership differential expression testing of three topics, corresponding to Figure 2e. Choroid plexus markers are highlighted for topic 3, dividing cell markers are highlighted in topic 4, and cell type-shared hypoxia-response genes are highlighted in topic 7.

Figure S4. Stressed cell identification and responses to treatment. **(a)** Fractional change in cell proportions classified as hypoxia-stressed and hyperoxia-stressed after high-oxygen treatment in coarsely classified cells. Note that elevated environmental oxygen reduces the fraction of cells classified as hypoxia-stressed. **(b)** Fractional change in cell proportions classified as hypoxia-stressed and hyperoxia-stressed after low- or high-oxygen treatment using fine-grained cell type classifications. **(c)** Canonical cell type markers are maintained in stressed cells. Cells classified as "stressed" retain key markers of their identities. **(d)** Stress-responsive cells account for many, but not all, of the DE genes (FDR<0.05 and fold-change>1.5) induced by hypoxia in the most responsive cell types. Censoring stressed cells reduces DE genes more than randomly censoring matched proportions of cells for indicated cell types.

Figure S5. Oxygen-responsive eGenes are less abundant in GTEx and include large numbers of GWAS genes. **(a)** Fractions of eGenes in each category classified as eGenes in GTEx cerebral cortex tissues. Oxygen-responsive eGenes boxed in red are less likely to be present in GTEx compared to eGenes boxed in blue (p=0.0083, one-sided paired Wilcoxon test). **(b)** Results as shown in (a) for eGenes identified from coarsely classified cell types (p=0.0039, one-sided paired Wilcoxon test). **(c)** Number of eGenes identified in each coarsely classified cell type, analogous to Figure 3a. **(d)** Number of eGenes identified in each coarsely classified cell type, analogous to Figure 3b. **(e)** Fractions of eGenes, identified in coarsely classified cell types, in

each category classified as eGenes in GTEx cerebral cortex tissues, analogous to Figure 3c (p=0.055, one-sided paired Wilcoxon test of oxygen-insensitive category [blue] against oxygen-responsive/undetected in normoxia category [dark red]). **(f)** Number of eGenes in each coarsely classified cell type which are the nearest gene to a genome-wide significant GWAS finding among 402 brain-related traits, analogous to Figure 4b. **(g)** Non-dynamic ("standard") eQTL effect of rs2008012 in dividing intermediate progenitor cells. This eQTL has an oxygen-responsive effect in immature neurons (Figure 4c).

Table S1. Results from *propeller* testing of oxygen treatment, sex, collection batch, and iPSC passage number on cell type proportions.

Table S2. Results from differential expression testing using *dream*.

Table S3. Gene lists used for identifying oxygen-responsive cells.

Table S4. Results of eQTL mapping and *mash* analysis.

Table S5. Rare variant genes used for analysis of eQTL results and rare variant gene-eQTL-GWAS phenotype triads.

Table S6. GWAS study accession identifiers (GWAS Catalog) used for analysis of eQTL results.

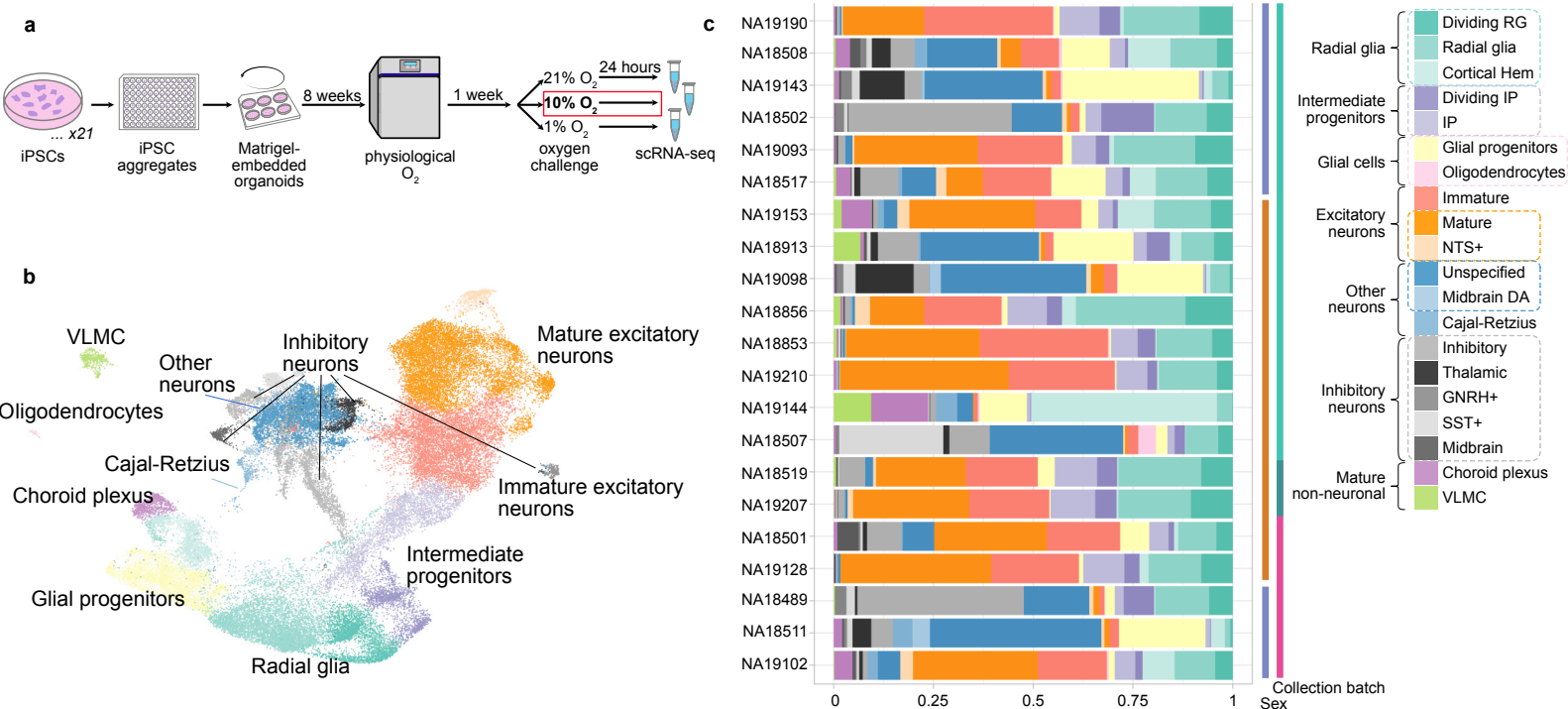
a
... x21
iPSCs
iPSC aggregates
Matrigel-embedded organoids
8 weeks
physiological O2
1 week
21% O2
24 hours
10% O2
1% O2
oxygen challenge
scRNA-seq
b
VLMC
Other neurons
Inhibitory neurons
Mature excitatory neurons
Oligodendrocytes
Cajal-Retzius
Choroid plexus
Immature excitatory neurons
Intermediate progenitors
Glial progenitors
Radial glia
c
NA19190
NA18508
NA19143
NA18502
NA19093
NA18517
NA19153
NA18913
NA19098
NA18856
NA18853
NA19210
NA19144
NA18507
NA18519
NA19207
NA18501
NA19128
NA18489
NA18511
NA19102
0
0.25
0.5
0.75
1
Collection batch
Sex
Radial glia
Dividing RG
Radial glia
Cortical Hem
Intermediate progenitors
Dividing IP
IP
Glial cells
Glial progenitors
Oligodendrocytes
Excitatory neurons
Immature
Mature
NTS+
Other neurons
Unspecified
Midbrain DA
Cajal-Retzius
Inhibitory neurons
Inhibitory
Thalamic
GNRH+
SST+
Midbrain
Mature non-neuronal
Choroid plexus
VLMC

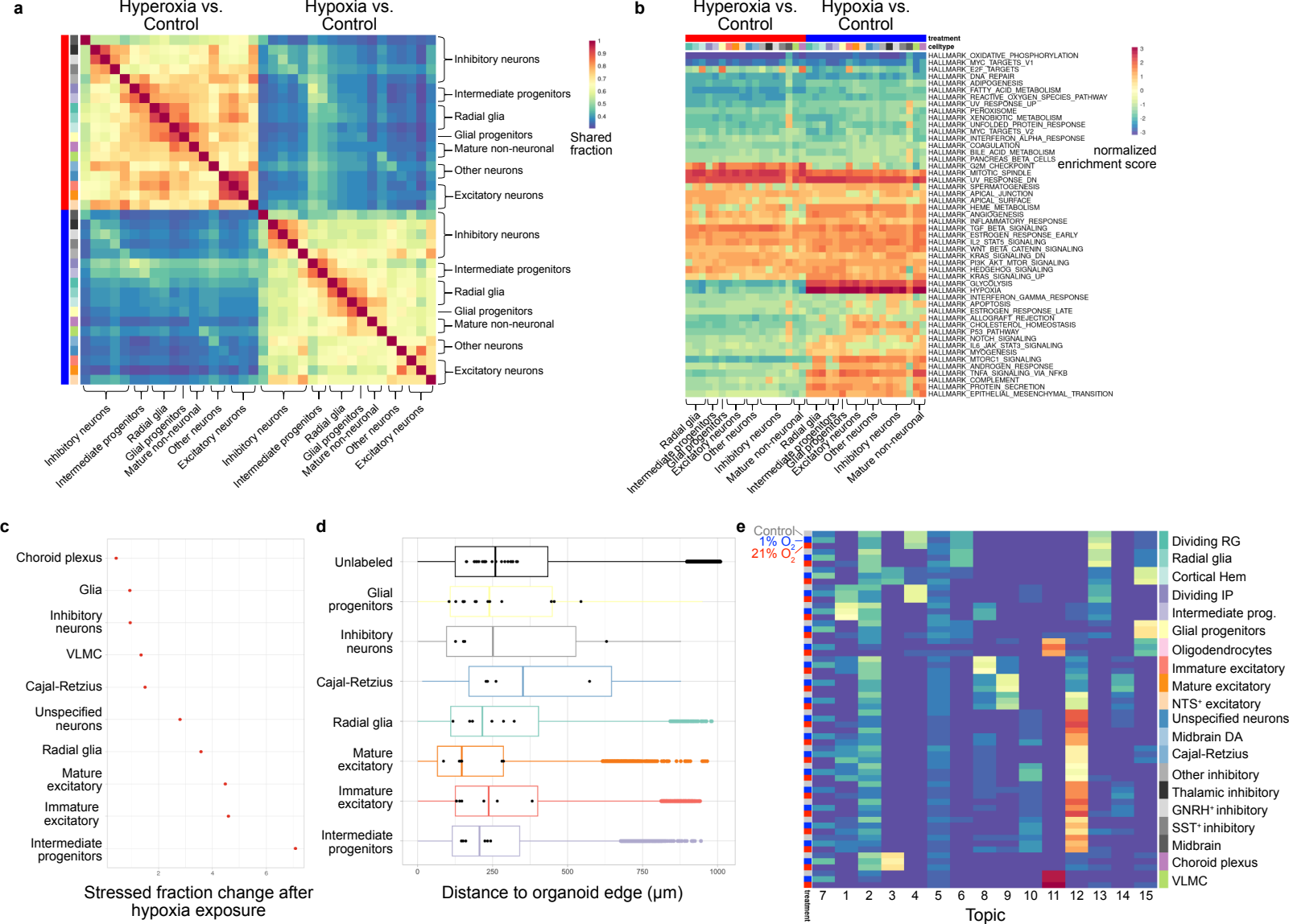
a
Hyperoxia vs. Control
Hypoxia vs. Control
Inhibitory neurons
Intermediate progenitors
Radial glia
Glial progenitors
Mature non-neuronal
Other neurons
Excitatory neurons
Shared fraction
b
Hyperoxia vs. Control
Hypoxia vs. Control
treatment
celltype
HALLMARK_OXIDATIVE_PHOSPHORYLATION
HALLMARK_MYC_TARGETS_V1
HALLMARK_E2F_TARGETS
HALLMARK_DNA_REPAIR
HALLMARK_ADIPOGENESIS
HALLMARK_FATTY_ACID_METABOLISM
HALLMARK_REACTIVE_OXYGEN_SPECIES_PATHWAY
HALLMARK_UV_RESPONSE_UP
HALLMARK_PEROXISOME
HALLMARK_XENOBIOTIC_METABOLISM
HALLMARK_UNFOLDED_PROTEIN_RESPONSE
HALLMARK_MYC_TARGETS_V2
HALLMARK_INTERFERON_ALPHA_RESPONSE
HALLMARK_COAGULATION
HALLMARK_BILE_ACID_METABOLISM
HALLMARK_PANCREAS_BETA_CELLS
HALLMARK_G2M_CHECKPOINT
HALLMARK_MITOTIC_SPINDLE
HALLMARK_UV_RESPONSE_DN
HALLMARK_SPERMATOGENESIS
HALLMARK_APICAL_JUNCTION
HALLMARK_APICAL_SURFACE
HALLMARK_HEME_METABOLISM
HALLMARK_ANGIOGENESIS
HALLMARK_INFLAMMATORY_RESPONSE
HALLMARK_TGF_BETA_SIGNALING
HALLMARK_ESTROGEN_RESPONSE_EARLY
HALLMARK_IL2_STAT5_SIGNALING
HALLMARK_WNT_BETA_CATENIN_SIGNALING
HALLMARK_KRAS_SIGNALING_DN
HALLMARK_PI3K_AKT_MTOR_SIGNALING
HALLMARK_HEDGEHOG_SIGNALING
HALLMARK_KRAS_SIGNALING_UP
HALLMARK_GLYCOLYSIS
HALLMARK_HYPOXIA
HALLMARK_INTERFERON_GAMMA_RESPONSE
HALLMARK_APOPTOSIS
HALLMARK_ESTROGEN_RESPONSE_LATE
HALLMARK_ALLOGRAFT_REJECTION
HALLMARK_CHOLESTEROL_HOMEOSTASIS
HALLMARK_P53_PATHWAY
HALLMARK_NOTCH_SIGNALING
HALLMARK_IL6_JAK_STAT3_SIGNALING
HALLMARK_MYOGENESIS
HALLMARK_MTORC1_SIGNALING
HALLMARK_ANDROGEN_RESPONSE
HALLMARK_TNFA_SIGNALING_VIA_NFKB
HALLMARK_COMPLEMENT
HALLMARK_PROTEIN_SECRETION
HALLMARK_EPITHELIAL_MESENCHYMAL_TRANSITION
normalized enrichment score
c
Choroid plexus
Glia
Inhibitory neurons
VLMC
Cajal-Retzius
Unspecified neurons
Radial glia
Mature excitatory
Immature excitatory
Intermediate progenitors
Stressed fraction change after hypoxia exposure
d
Unlabeled
Glial progenitors
Inhibitory neurons
Cajal-Retzius
Radial glia
Mature excitatory
Immature excitatory
Intermediate progenitors
Distance to organoid edge (μm)
e
Control
1% O2
21% O2
treatment
Dividing RG
Radial glia
Cortical Hem
Dividing IP
Intermediate prog.
Glial progenitors
Oligodendrocytes
Immature excitatory
Mature excitatory
NTS+ excitatory
Unspecified neurons
Midbrain DA
Cajal-Retzius
Other inhibitory
Thalamic inhibitory
GNRH+ inhibitory
SST+ inhibitory
Midbrain
Choroid plexus
VLMC
Topic

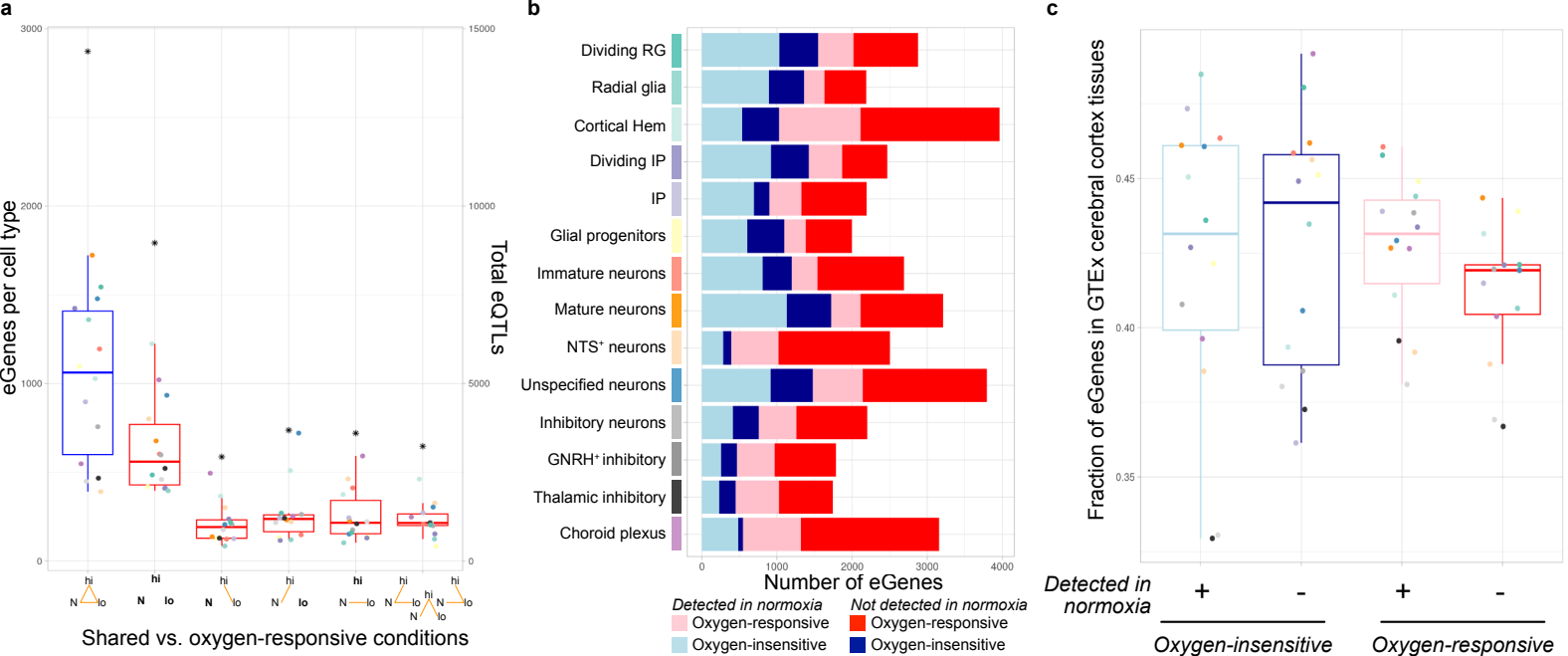
a
eGenes per cell type
Total eQTLs
3000
2000
1000
0
15000
10000
5000
0
hi
N
lo
Shared vs. oxygen-responsive conditions
b
Dividing RG
Radial glia
Cortical Hem
Dividing IP
IP
Glial progenitors
Immature neurons
Mature neurons
NTS+ neurons
Unspecified neurons
Inhibitory neurons
GNRH+ inhibitory
Thalamic inhibitory
Choroid plexus
0
1000
2000
3000
4000
Number of eGenes
Detected in normoxia
Oxygen-responsive
Oxygen-insensitive
Not detected in normoxia
Oxygen-responsive
Oxygen-insensitive
c
Fraction of eGenes in GTEx cerebral cortex tissues
0.45
0.40
0.35
Detected in normoxia
+
-
+
-
Oxygen-insensitive
Oxygen-responsive

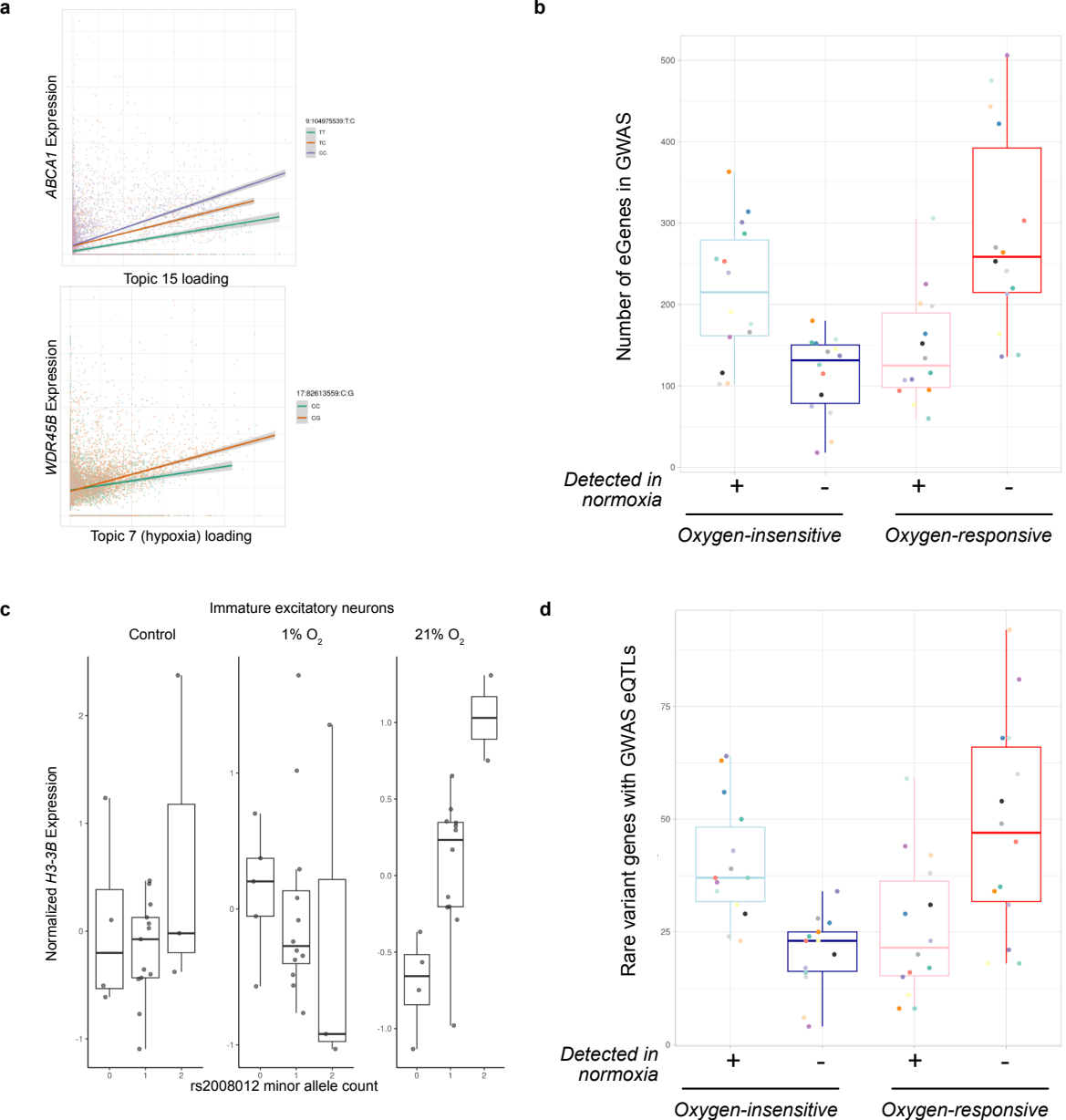
a
ABCA1 Expression
9:104975539:T:C
TT
TC
CC
Topic 15 loading
WDR45B Expression
17:82613559:C:G
CC
CG
Topic 7 (hypoxia) loading
b
Number of eGenes in GWAS
Detected in normoxia
+
-
+
-
Oxygen-insensitive
Oxygen-responsive
c
Immature excitatory neurons
Control
1% O2
21% O2
Normalized H3-3B Expression
rs2008012 minor allele count
d
Rare variant genes with GWAS eQTLs
Detected in normoxia
+
-
+
-
Oxygen-insensitive
Oxygen-responsive

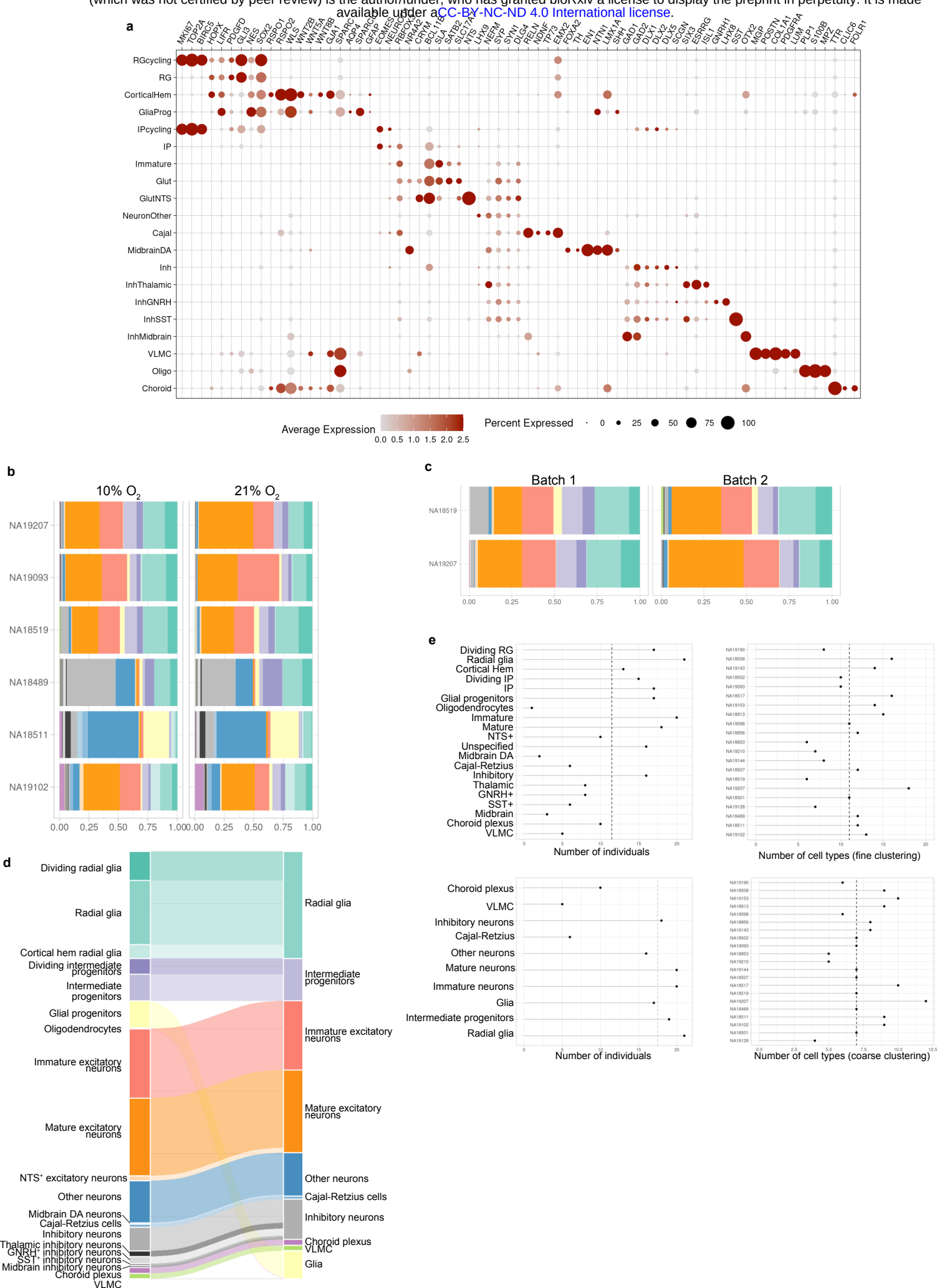

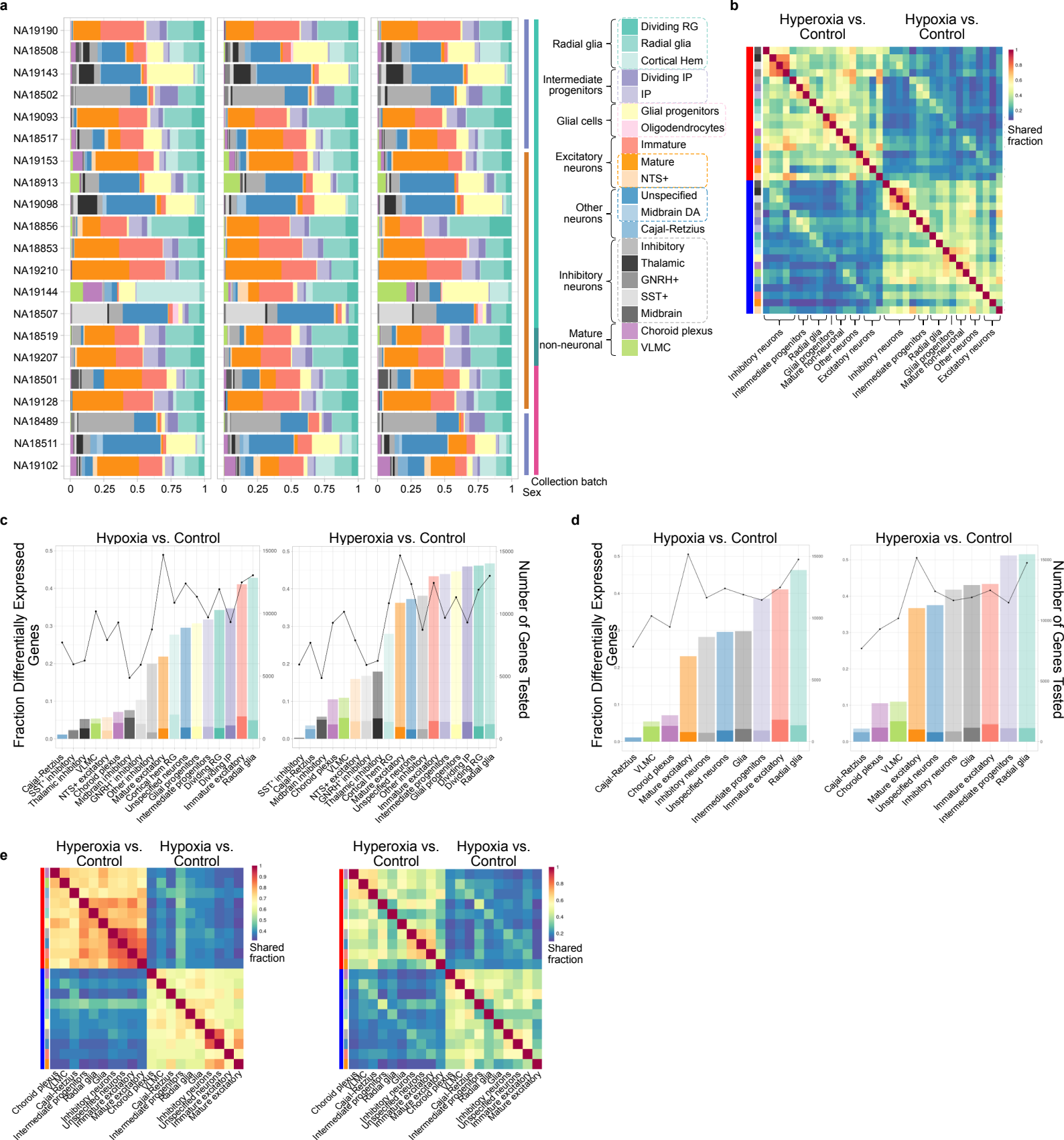
a
NA19190
NA18508
NA19143
NA18502
NA19093
NA18517
NA19153
NA18913
NA19098
NA18856
NA18853
NA19210
NA19144
NA18507
NA19519
NA19207
NA18501
NA19128
NA18489
NA18511
NA19102
0
0.25
0.5
0.75
1
Radial glia
Dividing RG
Radial glia
Cortical Hem
Intermediate progenitors
Dividing IP
IP
Glial cells
Glial progenitors
Oligodendrocytes
Excitatory neurons
Immature
Mature
NTS+
Other neurons
Unspecified
Midbrain DA
Cajal-Retzius
Inhibitory neurons
Inhibitory
Thalamic
GNRH+
SST+
Midbrain
Mature non-neuronal
Choroid plexus
VLMC
Collection batch
Sex
b
Hyperoxia vs. Control
Hypoxia vs. Control
Shared fraction
Inhibitory neurons
Intermediate progenitors
Radial glia
Glial progenitors
Mature non-neuronal
Other neurons
Excitatory neurons
c
Hypoxia vs. Control
Hyperoxia vs. Control
Fraction Differentially Expressed Genes
Number of Genes Tested
Cajal-Retzius
SST+ inhibitory
Thalamic inhibitory
VLMC
NTS+ excitatory
Choroid plexus
Midbrain inhibitory
GNRH+ inhibitory
Other inhibitory
Mature excitatory
Cortical hem
Unspecified neurons
Glial progenitors
Dividing IP
Dividing RG
Immature excitatory
Radial glia
d
Hypoxia vs. Control
Hyperoxia vs. Control
Fraction Differentially Expressed Genes
Number of Genes Tested
Cajal-Retzius
VLMC
Choroid plexus
Mature excitatory
Inhibitory neurons
Unspecified neurons
Glia
Intermediate progenitors
Immature excitatory
Radial glia
e
Hyperoxia vs. Control
Hypoxia vs. Control
Shared fraction
Choroid plexus
VLMC
Cajal-Retzius
Intermediate progenitors
Radial glia
Glia
Inhibitory neurons
Unspecified neurons
Immature excitatory
Mature excitatory

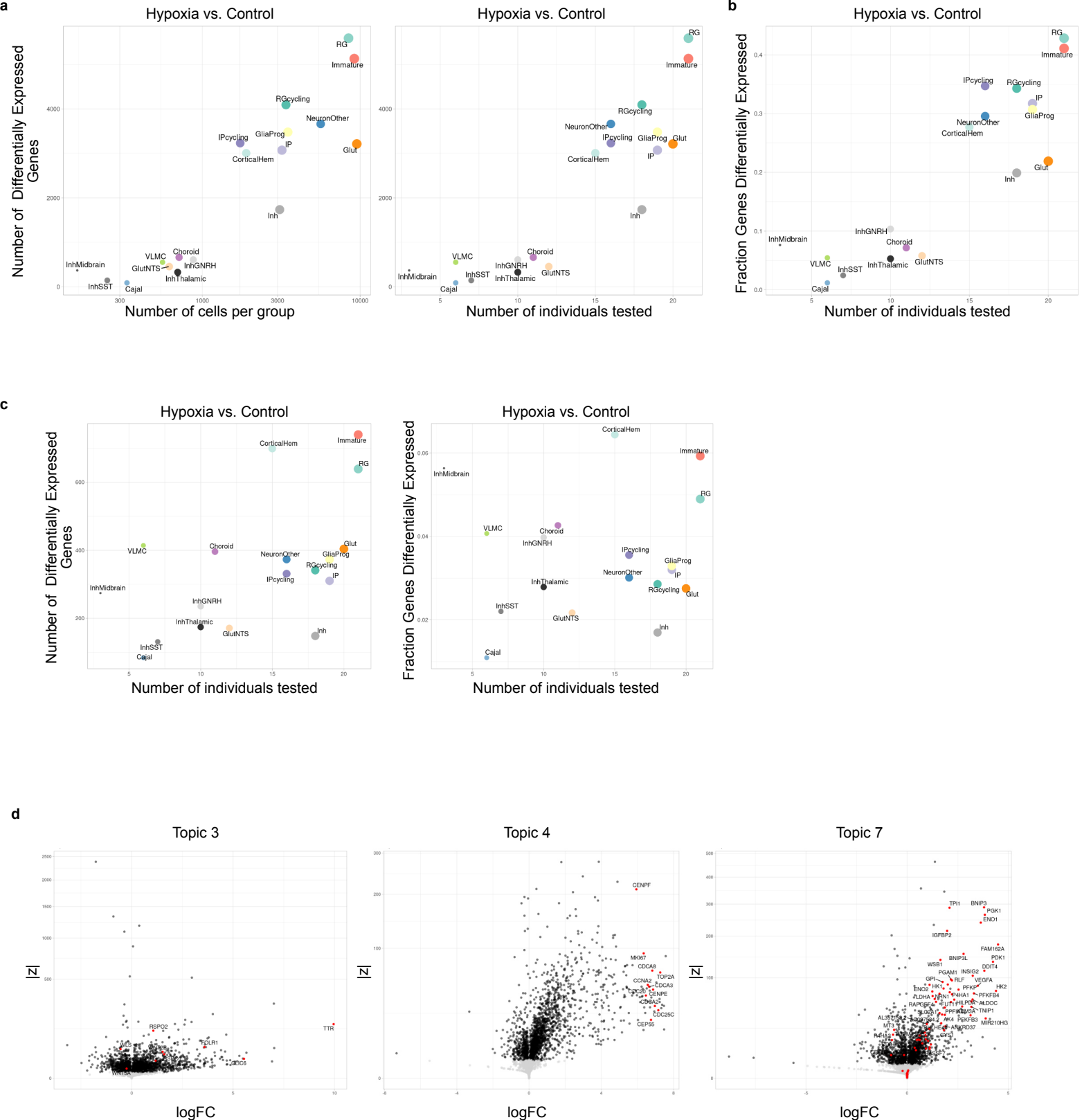
a
Hypoxia vs. Control
Number of Differentially Expressed Genes
Number of cells per group
RG
Immature
RGcycling
NeuronOther
IPcycling
GliaProg
IP
Glut
CorticalHem
Inh
Choroid
VLMC
InhMidbrain
GlutNTS
InhGNRH
InhThalamic
InhSST
Cajal
Hypoxia vs. Control
Number of individuals tested
b
Hypoxia vs. Control
Fraction Genes Differentially Expressed
Number of individuals tested
c
Hypoxia vs. Control
Number of Differentially Expressed Genes
Number of individuals tested
Hypoxia vs. Control
Fraction Genes Differentially Expressed
Number of individuals tested
d
Topic 3
Topic 4
Topic 7
|z|
logFC
CENPF
MKI67
CDCA8
TOP2A
CCNA2
CDCA3
CENPE
CDC25C
CEP55
TTR
RSPO2
TPI1
BNIP3
PGK1
ENO1
IGFBP2
FAM162A
PDK1
BNIP3L
DDIT4
VEGFA
HK2
PFKFB4
TNIP1
MIR210HG

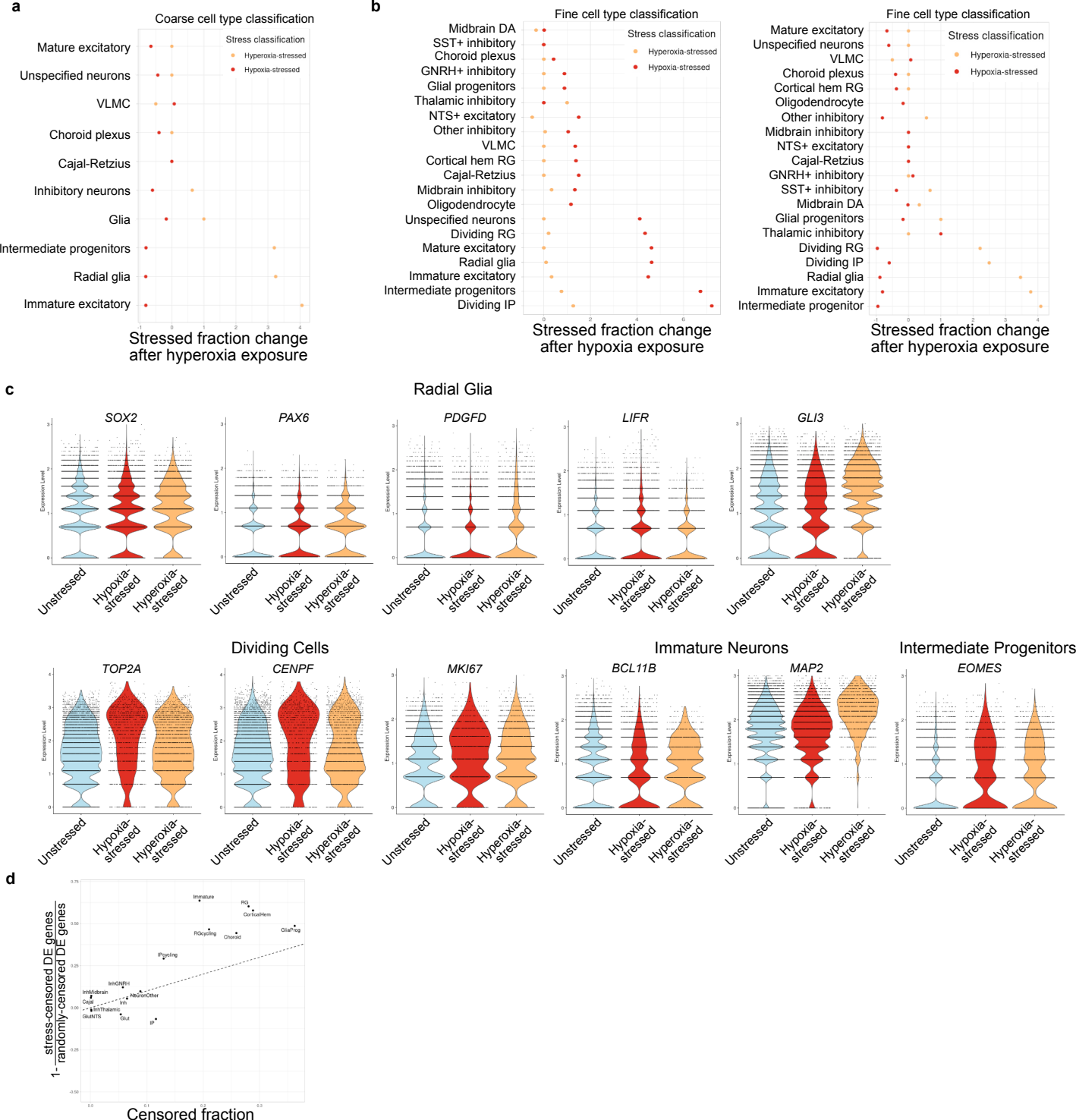
a
Coarse cell type classification
Stress classification
Hyperoxia-stressed
Hypoxia-stressed
Mature excitatory
Unspecified neurons
VLMC
Choroid plexus
Cajal-Retzius
Inhibitory neurons
Glia
Intermediate progenitors
Radial glia
Immature excitatory
Stressed fraction change after hyperoxia exposure
b
Fine cell type classification
Midbrain DA
SST+ inhibitory
Choroid plexus
GNRH+ inhibitory
Glial progenitors
Thalamic inhibitory
NTS+ excitatory
Other inhibitory
VLMC
Cortical hem RG
Cajal-Retzius
Midbrain inhibitory
Oligodendrocyte
Unspecified neurons
Dividing RG
Mature excitatory
Radial glia
Immature excitatory
Intermediate progenitors
Dividing IP
Stressed fraction change after hypoxia exposure
Fine cell type classification
Mature excitatory
Unspecified neurons
VLMC
Choroid plexus
Cortical hem RG
Oligodendrocyte
Other inhibitory
Midbrain inhibitory
NTS+ excitatory
Cajal-Retzius
GNRH+ inhibitory
SST+ inhibitory
Midbrain DA
Glial progenitors
Thalamic inhibitory
Dividing RG
Dividing IP
Radial glia
Immature excitatory
Intermediate progenitor
Stressed fraction change after hyperoxia exposure
c
Radial Glia
SOX2
PAX6
PDGFD
LIFR
GLI3
Expression Level
Unstressed
Hypoxia-stressed
Hyperoxia-stressed
Dividing Cells
TOP2A
CENPF
MKI67
Immature Neurons
BCL11B
MAP2
Intermediate Progenitors
EOMES
d
stress-censored DE genes
1 - randomly-censored DE genes
Censored fraction
Immature
RG
CorticalHem
RGcycling
Choroid
GliaProg
IPcycling
ImmGNRH
InhMidbrain
Cajal
ImmOther
Imm
InhThalamic
GlutNTS
Glut
IP

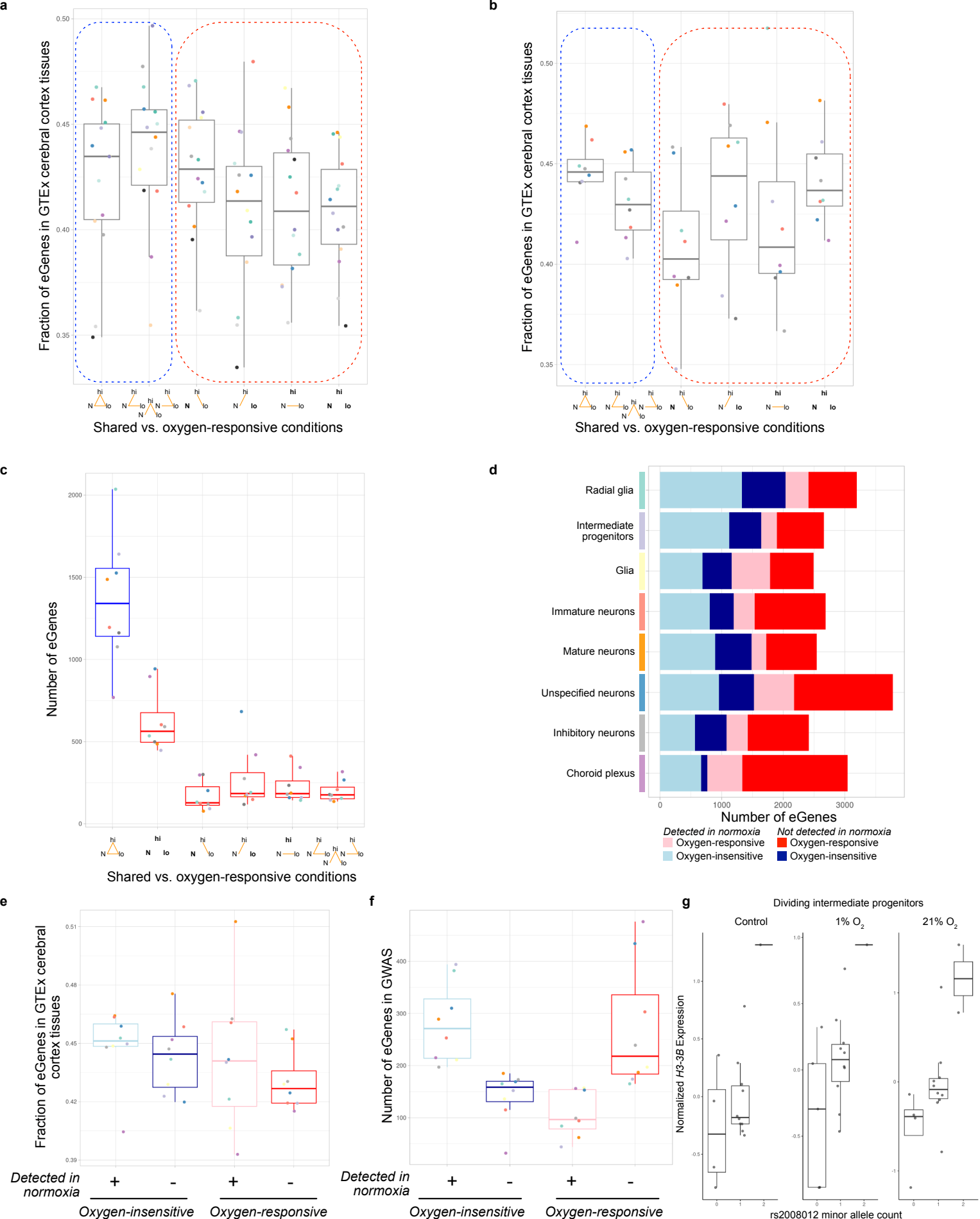
a
Fraction of eGenes in GTEx cerebral cortex tissues
Shared vs. oxygen-responsive conditions
b
Fraction of eGenes in GTEx cerebral cortex tissues
Shared vs. oxygen-responsive conditions
c
Number of eGenes
Shared vs. oxygen-responsive conditions
d
Radial glia
Intermediate progenitors
Glia
Immature neurons
Mature neurons
Unspecified neurons
Inhibitory neurons
Choroid plexus
Number of eGenes
Detected in normoxia
Oxygen-responsive
Oxygen-insensitive
Not detected in normoxia
Oxygen-responsive
Oxygen-insensitive
e
Fraction of eGenes in GTEx cerebral cortex tissues
Detected in normoxia
Oxygen-insensitive
Oxygen-responsive
f
Number of eGenes in GWAS
Detected in normoxia
Oxygen-insensitive
Oxygen-responsive
g
Dividing intermediate progenitors
Control
1% O2
21% O2
Normalized H3-3B Expression
rs2008012 minor allele count